Layer-by-Layer Modification of Electrospun Bipolar Membranes

Jansman, M.J. (Thijs)

Award date:
2024

Department of Chemical Engineering and Chemistry

Membrane Materials and Processes

Layer-by-Layer Modification of Electrospun Bipolar Membranes

Master Thesis

Mathijs Johannes Jansman

Supervisors:

Prof. Dr. Ir. Kitty Nijmeijer

Dr. Ing. Zandrie Borneman

Dr. Ir. Thijs de Groot

Dr. Ir. Menno Houben

Eindhoven, September 2023

(This page is left blank intentionally).

Abstract

Because of global warming and climate change a worldwide shift is seen from burning fossil fuels to the use of renewable energy. To reach the goal of becoming completely climate neutral by 2050, the share of renewables is expected to increase drastically. This leads to the inevitable electrification of the industry, where electricity becomes the main driving force for existing and emerging industrial processes. In many of such processes, bipolar membranes (BPMs) could play a promising role. BPMs are a type of ion exchange membrane that consist of a cation exchange layer (CEL) and an anion exchange layer (AEL), which are separated by an interface layer (IL) or bipolar junction. BPMs are able to facilitate the water dissociation (WD) reaction in the IL when a sufficient potential is applied. The in situ production of H^+ and OH^- ions enables BPMs to maintain a stable pH gradient across the membrane, making them a useful tool in many electrochemical applications, such as in flow batteries or water electrolysis. However, the currently available commercial BPMs lack the efficiency and mechanical stability required for these high current density operations. In this regard, electrospinning in combination with the incorporation of WD catalysts is suggested to improve both properties. Preparation of BPMs with electrospinning creates an entangled network between the CEL and AEL, which improves the mechanical properties, while it enhances WD by providing alternative pathways for the WD products to leave the junction. In this study, BPMs are fabricated using electrospinning, followed by hot pressing. The material used for the CEL is sulfonated poly(ether ether ketone) (SPEEK) and for the AEL the commercially available FAA-3 is used. The WD catalysts are introduced to the IL by layer-by-layer (LbL) modification of the electrospun SPEEK. With the LbL method, polyelectrolyte multilayers (PEMs) are deposited by alternating adsorption of polyethyleneimine (PEI) and polyacrylic acid (PAA). The growth of PEI and PAA multilayers can be controlled by varying external factors, such as the polyelectrolyte concentration, ionic strength and pH. The multilayer growth was monitored on a silicon wafer via optical fixed angle reflectometry. At a pH of 6.5, linear growth was observed for low ionic strengths (5 and 50 mM NaCl). Coating at a high ionic strength (500 mM NaCl) resulted in exponential growth of the multilayer, due to the screening of charges by salt ions and interdiffusion of the polyelectrolyte chains. This lead to significantly larger total adsorption values after deposition of the same number of layers. The pH could be used to vary the ionization degree of PEI and PAA. The ionization degree affects the diffusivity of PEI and PAA and dictates the type of multilayer growth. It was found that the multilayers grew linearly at high ionization degrees, while exponential growth was observed for low ionization degrees. Especially the ionization degree of PAA determined the growth behavior. The catalytic effect of PEI and PAA multilayers on WD was assessed electrochemically by recording polarization curves and measuring the permselectivity. The results showed that incorporation of low amounts of PEI and PAA already resulted in a significant reduction of the WD onset potential when compared to an electrospun BPM without catalyst. The best WD performance was found in BPMs with the highest catalyst loadings and where the PEI and PAA multilayers showed exponential growth. Similar results were observed during the permselectivity measurements, showing that the combination of electrospinning and the LbL modification of the IL with PEI and PAA multilayers is promising for the development of high performance BPMs.

Acknowledgements

Dear reader,

This thesis represents the work that I have been doing during my graduation project in the Membrane Materials and Processes (MMP) group at Eindhoven University of Technology (TU/e). When I started the Master program in the Molecular Systems and Materials Chemistry track, I had a clear vision for the direction I wanted to take. I was trying to find the interface between chemistry and sustainably energy applications. After talking to several professors, this proved to be harder than expected. Until I took the course Polymer Membranes for sustainable process applications from Kitty Nijmeijer, which offered exactly what I was looking for. In her group (MMP), I finished a small project in the form of a Capita Selecta under Menno Houben. Due to the interesting topic and pleasant collaboration I decided to stay for my graduation project. That is why I want to take this opportunity to thank Kitty Nijmeijer for letting me be a part of this amazing group. Of course I also want to thank her for taking the time to read and evaluate my work. In this regard I also want to thank Zandrie Borneman and Thijs de Groot for their supervision and evaluation of my graduation project. In particular, I want to thank Menno Houben, for having the patience to put up with me for more than a year. Your supervision, comments and company have been invaluable. Of course I would also like to thank the other members of the group, who have been supportive along the way. Furthermore, I would like to thank the students in the student office, who were always up for a rant while enjoying a nice cup of coffee. Finally, I would like to thank my family and friends, who have supported me unconditionally.

List of abbreviations

α	Degree of ionization
η_{WD}	Water dissociation overpotential
AEL	Anion exchange layer
AEM	Anion exchange membrane
$AlOH_3$	Aluminium hydroxide
ASR	Area specific resistance
BL	Bilayer
BPM	Bipolar membrane
c_{cr}	Critical salt concentration
CEL	Cation exchange layer
CEM	Cation exchange membrane
CO_2	Carbon dioxide
CRM	Chemical reaction model
EDBM	Electrodialysis with bipolar membranes
EDS	Energy dispersive X-ray spectroscopy
EFE	Electric field enhanced
GO	Graphene oxide
HCl	Hydrochloric acid
HER	Hydrogen evolution reaction
i_{lim}	Limiting current density
IEL	Ion exchange layer
IEM	Ion exchange membrane
IL	Interface layer
LbL	Layer-by-layer
Na_2SO_4	Sodium sulfate
NaCl	Sodium chloride
NaOH	Sodium hydroxide
OCV	Open circuit voltage
OER	Oxygen evolution reaction
PA	Polyanion
PAA	Polyacrylic acid
PC	Polycation
PE	Polyelectrolyte
PEI	Polyethyleneimine
PEM	Polyelectrolyte multilayer
PSS	Polystyrene sulfate
PZC	Point of zero charge
Q-PEC	Quasi-soluble polyelectrolyte complex
RH	Relative humidity
SCC	Soluble coacervate complexes
SCR	Space charge region
SEM	Scanning electron microscopy
SPEEK	Sulfonated poly(ether ether ketone)
SWE	Second Wien effect
U_{WD}	Water dissociation onset potential
WD	Water dissociation

Contents

Chapter 1. Introduction

The emission of greenhouse gases, such as methane and carbon dioxide (CO_2), is believed to be the root cause of global warming and climate change.[1] Since the Industrial Revolution, the atmospheric CO_2 concentration has risen from 280 ppm to 420 ppm (observed at Mauna Loa Observatory in Hawaii on March 15, 2023) and has caused an increase of the average global temperature of at least 1.1°C since 1880.[2–4] In order to limit the average global temperature increase to 1.5°C, it is required to reduce greenhouse gas emissions to 55% of the 2010 level by 2030 and net zero emissions need to be achieved by 2050.[5,6] To reach these goals, a worldwide shift is seen from burning fossil fuels to renewable energy sources.[7] The biggest share is occupied by intermittent sources like wind and solar.[8] To compensate for the intermittent availability, long-term storage solutions are required, like hydrogen based energy storage or flow batteries.[9,10] Besides energy storage, the industry has to make a transition towards using electricity as a power source. This makes electrochemical processes like electrodialysis, water electrolysis or CO_2 reduction attractive applications to use renewable energy for.[11] Figure 1.1 shows a schematic overview of how renewable energy driven electrochemical processes would integrate in society and industry. Bipolar membranes (BPMs) could play a crucial role in the "electrification" of the industry.

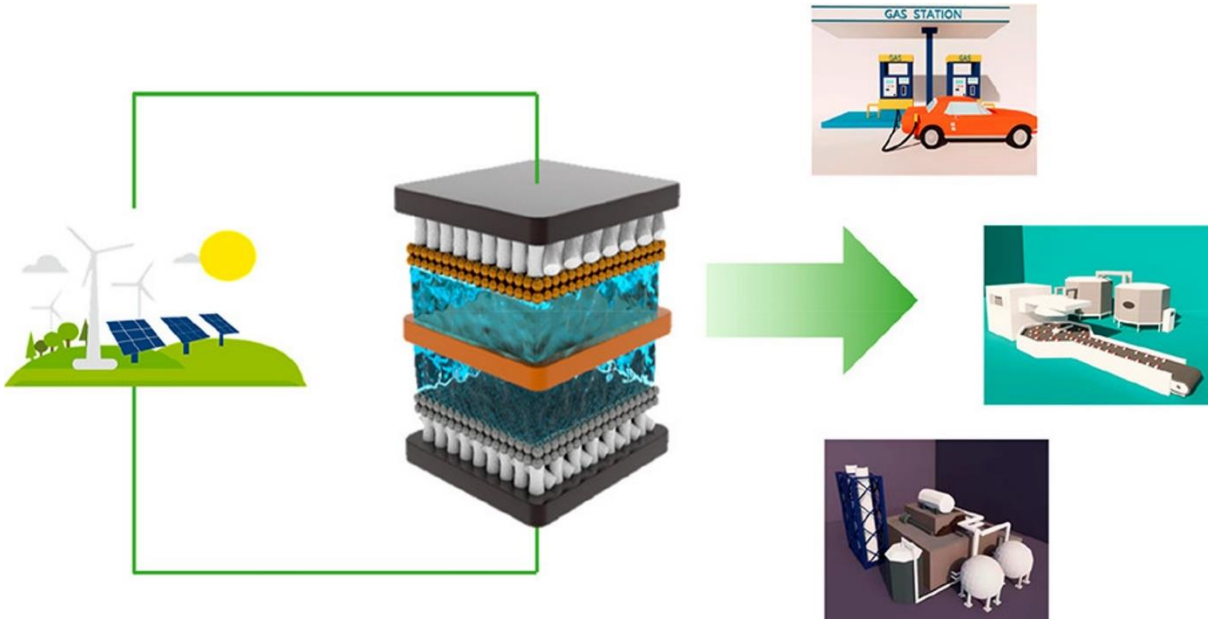

Figure 1.1 Schematic overview of how electrochemical processes driven by renewable energy could help with the electrification of the industry. Adapted from Xia et al.[11]

The BPM is the laminated structure of a cation (CEM) and anion exchange membrane (AEM) and has the ability to dissociate water into H^+ and OH^- ions when a sufficient potential is applied. They were traditionally developed for the production and recovery of acids and bases via a process called electrodialysis with BPMs (EDBM). In EDBM, a BPM is combined with conventional electrodialysis to produce acids and bases from their corresponding salts.[12,13] The largest share is occupied by the production of HCl and NaOH from desalination brines.[14] EDBM is also used for the recovery of other inorganic acids and bases, such as phosphoric acid, sulfuric acid, calcium hydroxide and ammonium hydroxide from waste streams.[15,16] Besides the (re)generation of inorganic acids and bases, EDBM is also used extensively for the production and purification of organic acids, such as citric acid[17,18], lactic acid[19,20], acetic acid[21] and tartaric acid[21,22] from fermentation broths and waste waters. More recently, BPMs are increasingly used in electrochemical energy applications, like CO_2 reduction[23] and

electrolysis[24], fuel cells[25], (acid-base) flow batteries[26–28] and water electrolysis.[29] The benefit of using a BPM in these applications is that, because of the ability to dissociate water into protons and hydroxide ions, a BPM is able to maintain a pH gradient across the membrane. A monopolar membrane limits the operation to either an acidic (CEM) or basic (AEM) environment and therefore restricts the electrode materials and catalysts that can be used. The pH gradient established by a BPM allows the electrode half-reactions to occur in a favorable pH environment for each reaction. This reduces the overpotential for the anodic and cathodic reactions while it also allows the use of (earth-abundant) catalysts that are optimal for the respective reaction.[30–32] However, BPM performance has to be improved before they can be implemented in these technologies on an industrial scale. Where state-of-the-art BPMs show water dissociation (WD) overpotentials (η_{WD}) greater than 100 mV at current densities of ~20 mA cm^{-2}, η_{WD} smaller than 100 mV at current densities of 1 to 2 A cm^{-2} are required to become economically feasible.[33] Another common known problem is that BPMs tend to delaminate when operated under high current densities or when water is recombined at the interface.[34–37] Therefore, the preparation of more mechanically robust BPMs is required.

The mechanical stability of BPMs can be improved by preparing them via electrospinning. Electrospinning is a technique where polymer nanofibers are produced under a strong electric field.[38] The nanofibers create an entangled network, physically linking the two layers of the BPM.[35] Several researchers have used electrospinning for BPM fabrication and all showed excellent mechanical stability.[35,36,39] To further improve BPM performance and reduce η_{WD}, the WD reaction rate must be accelerated. The addition of WD catalysts can significantly increase the BPM performance compared to BPMs without.[40,41] Shen et al. air sprayed aluminum hydroxide particles during the electrospinning of their BPM.[35] Chen et al. added graphene oxide particles to their BPM via a similar method.[36] Al-Dhubhani et al. dissolved a polymer catalyst in one of their electrospinning solutions to disperse it into the polymer nanofibers. The abovementioned methods all showed an improvement of the BPM performance, however, precise control of the thickness and architecture of the catalyst layer is unsatisfactory. A method that can provide this control is the layer-by-layer (LbL) method. The LbL method allows the growth of polyelectrolyte multilayers (PEMs) by alternating the deposition of oppositely charged polyelectrolytes (PEs).[42] The amount of PE and the PEM thickness can be controlled via external factors, such as pH and salt concentration.[43] This allows for the deposition of thin catalyst layers with properties controllable to the nanoscale.[44]

In this work, electrospinning will be used to fabricate BPMs with an entangled interface. PE catalyst layers will be deposited onto the electrospun nanofibers via the LbL method. The effect of the PE concentration, ionic strength and pH of the coating solutions on the PEM growth, as well as the BPM performance will be determined. The WD performance of the LbL modified BPMs will be assessed via electrochemical characterization techniques. Chapter 2 will provide the fundamentals of WD in BPMs and the LbL technique. The experimental part of this thesis will be discussed in Chapter 3. Here, the PEM growth study, the BPM fabrication and characterization will be discussed separately. The experimental findings will be discussed in Chapter 4. In Chapter 5 the conclusions that are drawn from the results will be summarized. Chapter 6 will provide recommendations for future work.

Chapter 2. Theoretical Background

2.1. Ion exchange membranes

Bipolar membranes (BPMs) are a type of ion exchange membrane (IEM). IEMs are semi-permeable membranes containing charged groups fixed to a polymer matrix. These fixed charges allow for the selective transport of oppositely charged ions, while they reject ions of the same charge.[45]There are two types of monopolar IEMs: the cation exchange membrane (CEM) and the anion exchange membrane (AEM). They are called monopolar, because all fixed charges in the polymer matrix are either positive or negative. A CEM, containing fixed, negatively charged groups, has selective transport of cations and rejects anions. The AEM has fixed, positively charged groups and selectively permeates anions, while rejecting cations. The extent to which ions of the same charge are blocked is called the permselectivity.[45] The transport of ions through IEMs is schematically shown in Figure 2.1. Commercial CEMs and AEMs often contain sulfonic acid and quaternary ammonium as charged functional groups, respectively. Because these groups are strong acids and bases the completely ionize in water and can therefore reach high ion conductivities.[45–48]

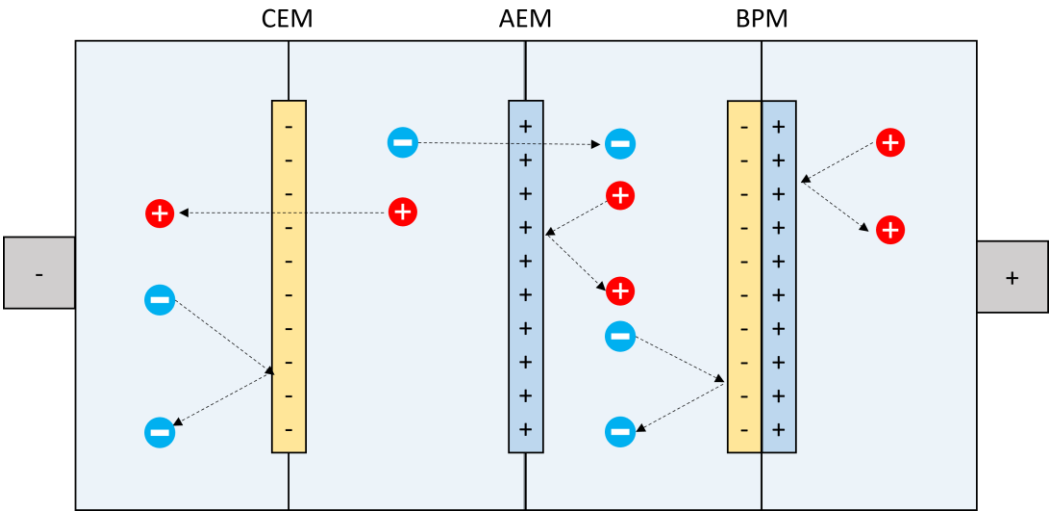

Figure 2.1 Schematic illustration of a cation exchange membrane, an anion exchange membrane and a bipolar membrane.

A BPM is a laminated structure of a CEM and an AEM. They consist of a cation exchange layer (CEL) and an anion exchange layer (AEL). The region at the interface of these two ion exchange layers (IELs) is called the interface layer (IL) or bipolar junction. Whereas monopolar IEMs are meant to transport ions from one compartment to another, BPMs are supposed to repel all charged species. This is also illustrated in Figure 2.1. Instead, a BPM is meant to facilitate the water dissociation (WD) reaction. The function of a BPM in an electrochemical cell depends on its orientation with respect to the electrodes. When the CEL faces the cathode (-) and the AEL faces the anode (+), WD occurs at the IL when a sufficient potential difference is applied. The WD products, H^+ and OH^-, permeate through the CEL and AEL, respectively, and migrate towards the cathode and anode. This mode of operation is called reverse bias and is schematically shown in Figure 2.2a. When the BPM is oriented such that the AEL faces the cathode and the CEL faces the anode, the BPM operates in forward bias. In forward bias, H^+ and OH^- ions migrate towards the IL and water recombination occurs. This is shown in Figure 2.2b. The main function of a BPM is to perform the WD reaction. Therefore, the following section will discuss the mechanism behind WD in BPMs under reverse bias.

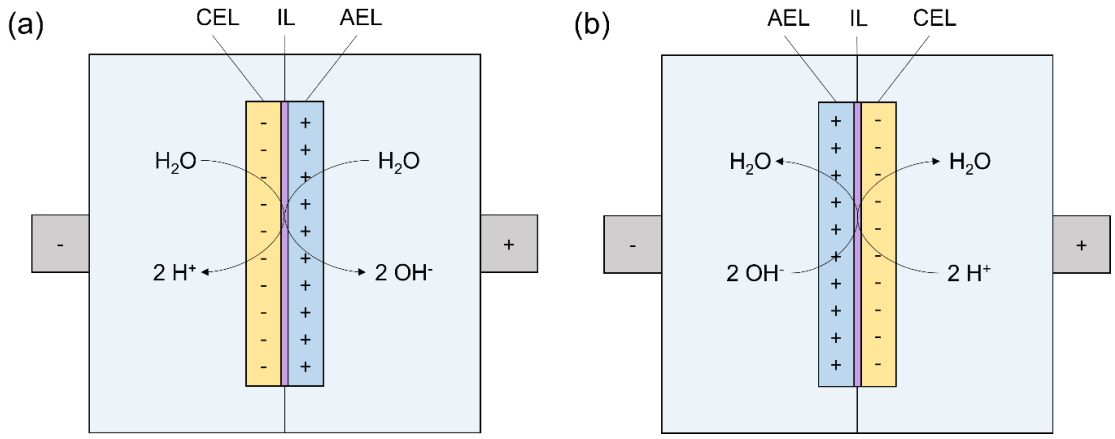

Figure 2.2 Schematic illustration of the function of a bipolar membrane under (a) reverse bias and (b) forward bias.

2.2. Water dissociation in bipolar membranes

The operation of BPMs under reverse bias is best explained by their current – voltage behavior. Figure 2.3a shows a typical polarization curve of a BPM in a salt-containing aqueous solution under reverse bias. The curve can be divided into three regions: (I) the Ohmic region, (II) the limiting region and (III) the overlimiting region. In the Ohmic region the potential increases linearly as a function of current density. As Figure 2.3b shows, the current in this region is mainly driven by co-ion transport across the membrane due to the imperfect permselectivity of the IELs. In the limiting region, salt ions migrate away from the IL and towards the anode and cathode until all salt ions are removed. At this point the limiting current density (i_{lim}) is reached and the resistance increases drastically, resulting in a sharp potential drop. The value of i_{lim} is considered to be a measure of the permselectivity of the BPM.[44,49–51]

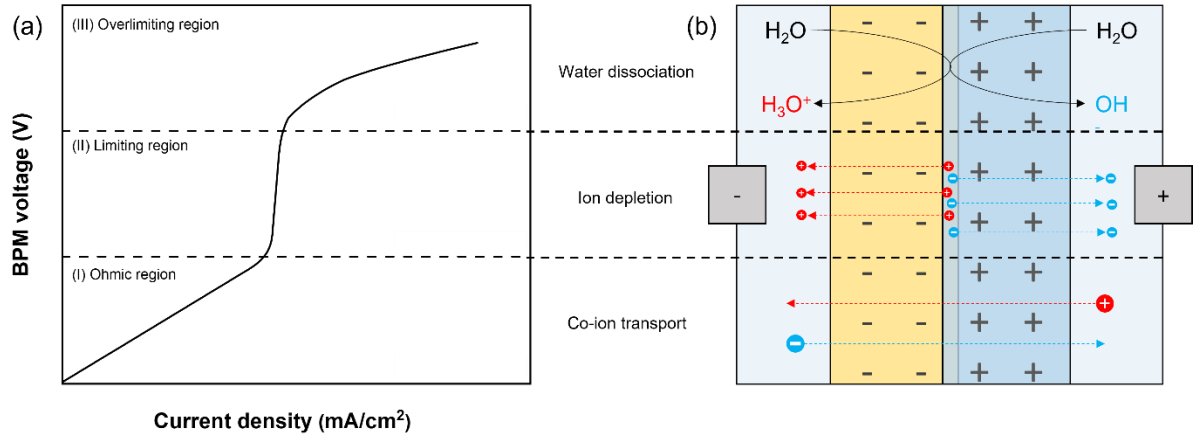

Figure 2.3 Schematic overview of (a) a typical polarization curve of a BPM in a salt-containing solution under reverse bias and (b) the corresponding transport of ions.

Beyond i_{lim}, in the overlimiting region, the only charge carriers left to sustain the current are protons and hydroxyl ions. These are available in low concentrations, even in deionized water.[50] Protons and hydroxyl ions that are removed from the IL are continuously replenished by the water dissociation equilibrium, according to Eq. 2.1.

$$H_2O \rightleftharpoons H^+ + OH^- \qquad \text{Eq. 2.1}$$

The minimum amount of energy that is theoretically required to convert one mole of water into protons and hydroxyl ions can be determined from the following relation:

$$G_0 = -RTln(K_w) = -zFE_0 \quad \text{Eq. 2.2}$$

Here, G_0 is the Gibb's free energy, R the universal gas constant (8.3145 J mol^{-1} K^{-1}), T the absolute temperature in K, z the ion valance, F the Faraday constant (96 485 C mol^{-1}) and E_0 the theoretical potential drop required to initiate the WD reaction. K_w is the WD equilibrium constant and is given by

$$K_w = \frac{[H^+][OH^-]}{[H_2O]} \quad \text{Eq. 2.3}$$

Using Eq. 2.2, the theoretically required water dissociation energy G_0 is determined to be 0.0222 kWh mol^{-1} under standard conditions. The necessary potential drop required to initiate WD E_0 is calculated to be -0.828 V.[50,51]

The WD rate in free solution ($2.5 \cdot 10^{-5}$ s^{-1}) is significantly lower than the rate of water formation ($1.1 \cdot 10^{11}$ M^{-1} s^{-1}) in the absence of an applied electric field.[52,53] When the potential drop across the BPM exceeds E_0, however, the rate of WD is observed to increase significantly (10^4 – 10^6 times).[51] The enhancement of the WD rate is described by two models: electric field enhanced (EFE) WD via the second Wien effect (SWE) and enhancement according to the chemical reaction model (CRM).[54,55]

2.2.1. Second Wien effect

When a BPM is under conditions where its functional groups are completely ionized, an electric field is generated between the CEL and AEL. This electric field drives the extraction of the mobile counterions in the IL, making it almost completely devoid of mobile ions.[56] This mobile-ion-free region is called the space charge region (SCR). The charge separation over this thin SCR (a few nm) produces an extremely high electric field up to 10^8 V m^{-1}. The SWE describes the influence of a strong electric field on the dissociation constants of weak electrolytes.[57] In the case of BPMs, water inside the IL is assumed to be a weak electrolyte. The WD rate increases exponentially with the strength of the electric field, while the water recombination rate remains constant.[58] According to the SWE, the ratio of the dissociation rate constant under the influence of an electric field ($k_{d(E)}$) over the dissociation rate constant without an electric field (k_d) can be determined via:

$$\frac{k_{d(E)}}{k_d} = \left(\frac{2}{\pi}\right)^{1/2} (8b)^{-3/4} e^{(8b)^{1/2}} \quad \text{Eq. 2.4}$$

With

$$b = 0.09636 \frac{E}{\varepsilon_r T^2} \quad \text{Eq. 2.5}$$

In Eq. 2.5, E is the electric field intensity in V m^{-1}, ε_r the relative permittivity (-) and T the temperature in K. Substituting the high electric field strength in this equation results in a $\frac{k_{d(E)}}{k_d} \approx 10^7$. This increase in the dissociation constant of water might explain the high water dissociation rate found in the i-V curves of the BPM. However, experimentally higher water dissociation rates have been observed than

predicted by just the SWE.[51,59,60] This observation has led to believe that an additional mechanism, namely the CRM, is contributing to WD in BPMs.

2.2.2. Chemical reaction model

According to the CRM, WD occurs via catalytic protonation – deprotonation reactions with ionic functional groups in the IL.[53] In the case of weakly basic functional groups, Simons[53] proposed the following mechanism:

$$B + H_2O \rightleftharpoons BH^+ + OH^- \quad \text{Eq. 2.6}$$

$$BH^+ + H_2O \rightleftharpoons B + H_3O^+ \quad \text{Eq. 2.7}$$

In Eq. 2.6 and Eq. 2.7, B represents a neutral base and BH^+ its conjugate acid. Here, BH^+ is the catalytic center (fixed charged groups on the AEL). In the case of a weak acid, the mechanism looks as follows:

$$A^- + H_2O \rightleftharpoons AH + OH^- \quad \text{Eq. 2.8}$$

$$AH + H_2O \rightleftharpoons A^- + H_3O^+ \quad \text{Eq. 2.9}$$

Where AH is the neutral acid and A^- its conjugate base. Here, A^- is the catalytic center (fixed charged groups in the CEL). Because basic groups tend to remain in the protonated form and acidic groups like to remain in the deprotonated form, Eq. 2.7 and Eq. 2.8 are the rate limiting steps in the protonation – deprotonation reactions.[61] The catalytic activity of the ionic functional groups is determined by the rate constants of the rate limiting (k_{lim}) steps of the protonation – deprotonation reactions. The identity of the ionic functional groups therefore affects the catalytic effect on the WD rate. Zabolotskii et al. drafted a table with experimental values of k_{lim} for some frequently used ionic functional groups in BPMs, where higher values for k_{lim} correspond to higher catalytic activities.[62] The values for k_{lim} are summarized in Table 2.1. Just like their monopolar counterparts, the most common functional groups found in the IELs in BPMs are sulfonic acid and quaternary ammonium groups.[40,41] As can be seen in Table 2.1, the catalytic activity of these functional groups is nearly nonexistent. Therefore, a thin layer containing a catalyst with weakly basic or acidic functional groups is often introduced to the IL to increase the WD performance.[63]

Table 2.1 Rate constants for the rate limiting step of the protonation – deprotonation reactions between water and some commonly used ionogenic functional groups in bipolar membranes.[52]

Functional group	$-N^+(CH_3)_3$	$-SO_3H$	$-PO_3H_2$	$=NH_2^+$, $-NH_3^+$	$\equiv NH^+$	$-COO^-$	$-PO_3H^-$
k_{lim} (s^{-1})	0	$3 * 10^{-3}$	$3 * 10^{-2}$	10^{-1}	1	10	10^2

2.3. Interface layer optimization

The use of a catalyst becomes imperative for a BPM to achieve optimum WD activity. However, incorporation of a catalyst layer in the bipolar junction might induce an opposing effect on the EFE WD. As the thickness of the catalyst layer increases, the strength of the electric field decreases and a trade-off arises between catalysis and EFE. Yan et al.[64] investigated the balance between the influence of a catalyst layer on the electric field by modifying BPMs with an increasing number of graphene oxide (GO) layer in the junction. They found that the WD rate constant increased with increasing

potential, indicating that WD is enhanced by the electric field regardless of the presence of a catalyst. Addition of more catalyst enhanced the WD performance, indicating that the catalyst promotes the WD reaction. However, the region in the bipolar junction that gets depleted of mobile ions under high reverse bias was found to get smaller as more catalyst was added. The presence of the catalyst layer drastically increased the flux of H^+ and OH^- ions, which partially compensate the unbalanced fixed charges on the AEL and CEL. This resulted in a decrease of the electric field strength and thus decreased the contribution of EFE on the acceleration of WD according to the SWE. Their research did however show that WD acceleration via catalysis is more important than EFE in case high current operation and high H^+ and OH^- fluxes are desirable.

Nonetheless, the amount cannot be increased indefinitely. Chen et al.[65] found a U-shaped dependance of the WD performance on the catalyst loading, especially at higher current densities. The WD performance initially increased with increased loadings, but the performance then decreased as the catalyst loadings increased further. They reasoned that the thicker catalyst layer increased the ionic resistance across the BPM junction, which decreased the overall WD performance despite the larger catalytic site density. Ideally, a catalyst should applied as a thin layer with a high active site density, so that the acceleration of WD via EFE and catalysis can work in tandem.

Next to the functionality of the catalytically active sites and the catalyst loading, the location of the catalyst was found to influence the acceleration of WD. Oener et al.[33] conducted a comprehensive study on the WD activity of various metal oxides in the IL. They systematically varied the WD catalyst in one layer, while using a chemically stable catalyst in the other layer. The WD activity was compared to the point of zero charge (PZC) of the metal oxides. It was found that integrating a catalyst with an acidic PZC in the CEL and a catalyst with a basic PZC in the AEL resulted in optimum WD performance. They also concluded that integrating a WD catalyst with a range or "spectrum" of pK_a values could significantly improve WD performance, so that WD can occur via both the weak base (Eq. 2.6 and Eq. 2.7) and the weak acid mechanism (Eq. 2.8 and Eq. 2.9).

Besides the addition of catalysts to the junction, the morphology of the IL also plays a crucial role in the performance of a BPM. The structure of the junction highly depends on the fabrication method. Historically, BPMs have been prepared via lamination of pre-existing casted anion and cation exchange membranes.[32,66] This preparation method yields a BPM with a smooth interface, as depicted in Figure 2.4a. The transition from the CEL to the AEL is abrupt and leads to a strong electric field in the junction. However, BPMs with a smooth IL are known to delaminate when operated at high current densities[34] or at high catalyst loadings,[36] compromising the performance of the BPM. The mechanical stability of a BPM can be improved by increasing the surface contact area in the IL. By mechanically processing a pre-casted IEL before casting the second layer a corrugated interface is obtained (Figure 2.4b).[67] The enlarged surface area increases adhesion, however, the transition from CEL to AEL is less abrupt. This causes the electrostatic potential between the CEL and AEL to be more spread out across the junction, resulting in a decrease of the electric field strength.[68] An IL with an even higher surface area is obtained in BPMs with an electrospun junction (Figure 2.4c). With electrospinning, an entangled network of anion and cation exchange fibers is obtained, drastically increasing adhesion between the AEL and CEL.[35] The opposite charges on the ionomer nanofibers in the entangled network cancel each other out, essentially introducing a neutral layer in the junction, causing a decrease of the electric field strength. However, the randomly distributed fibers provide unobstructed pathways for the WD reaction products to reach the respective IELs, while also minimizing water depletion, drastically enhancing WD performance.[35]

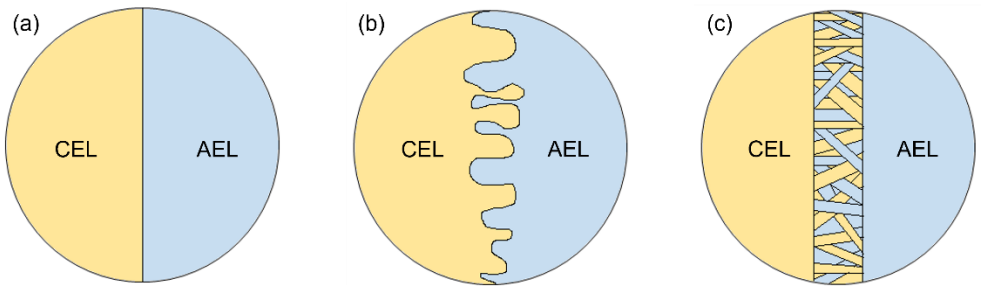

Figure 2.4 Types of IL structure: (a) smooth, (b) corrugated, (c) electrospun.

Shen et al.[35] were the first to fabricate BPMs with a 3D junction via dual nanofiber electrospinning of SPEEK and QPPO as the CEL and AEL, respectively. Aluminum hydroxide ($Al(OH)_3$) particles were added to the IL as a WD catalyst. The 3D junction was fabricated by first spinning a SPEEK nanofiber mat. Then, SPEEK and QPPO were spun simultaneously on top of the existing SPEEK mat, while concurrently air-spraying an aqueous $Al(OH)_3$ solution until a loading of 1.5 mg cm^{-2} was reached. Finally, a QPPO layer was spun on top of the junction mat. The electrospun mats were then hot pressed at 140 MPa at 121°C for 30 minutes, yielding a dense BPM with a high interfacial area junction of about 10 µm in thickness. Polarization curves were recorded by applying a steady state current and measuring the voltage drop across the BPM in 0.5 M Na_2SO_4 solution. The 3D BPM was compared to an electrospun BPM with a 2D junction and to a commercial BPM by Fumatech GmbH (Fumasep® FBM). Their 3D BPM showed a reproducible WD onset potential in the 0.83 – 0.90 V range and current densities were reached of 1100 mA cm^{-2} at a potential drop of only 1.5 V. The 3D BPM showed no signs of degradation at these current densities, whereas the Fumasep® FBM was damaged irreversibly at current densities of 600 mA cm^{-2}.

Following the same dual fiber electrospinning method, Chen et al.[36] prepared 3D junction BPMs from Nafion and an in-house synthesized perfluorinated AEM ionomer as the CEL and AEL, respectively. Unlike Shen et al., Chen et al. electrosprayed graphene oxide (GO) as a catalyst during the electrospinning of the 3D junction. After exposing the mats to IPA vapor and hot pressing, a dense BPM was yielded with a 3D junction of about 3 – 5 µm. In their study, a 2D BPM with and without catalyst was compared to the 3D BPM. The voltage of the catalyzed 2D BPM at 100 mA cm^{-2} had decreased by more than 75% compared to the uncatalyzed 2D BPM, emphasizing the importance of a WD catalyst. With the same catalyst loading, the 3D BPM showed even better performance with a potential of 1.5 V at 500 mA cm^{-2}. The mechanical stability the electrospun junction provides was demonstrated in a stability test, where the potential across the 3D BPM increased by 7.5% after 14 hours of operation at 500 mA cm^{-2}, while the potential across the Fumasep® FBM increased by 10%.

In a similar study, Al-Dhubhani et al.[39] systematically studied the effect of a dual nanofiber electrospun 3D junction and the role of a WD catalyst on the WD rate by comparing 3D BPMs with and without catalysts to 2D BPMs with and without catalysts. Dual-fiber electrospinning was again used for the preparation of 3D junction BPMs, this time from SPEEK and Fumion® FAA-3 as the CEL and AEL, respectively. Their study differed, however, in the way the catalyst was introduced. Instead of electrospraying catalytically active particles, a polymeric catalyst was dispersed within the FAA-3 nanofibers. Poly(4-vinlypyrrolidine) (P4VP) was added to the FAA-3 dope solution in different weight concentrations. This method of catalyst immobilization should prevent unwanted catalyst leakage and decreases the risk of delamination that might occur in BPMs with catalysts added via electrospraying. Their electrospun 3D junction BPMs outperformed the laminated 2D junction BPMs by a large margin. Increasing the P4VP loading in the 3D BPMs also showed a significant performance increase.

Inspired by the works described above, this study will use electrospinning for the preparation of BPMs with an entangled 3D junction. Sulfonated poly(ether ether ketone) (SPEEK) will be used as the CEL material and its structure is shown in Figure 2.5. For the production of the AEL, the commercially available Fumion® FAA-3 will be used. The exact structure of FAA-3 has not been disclosed, but it consists of a polyaromatic polymer functionalized with quaternary ammonium groups.[69]

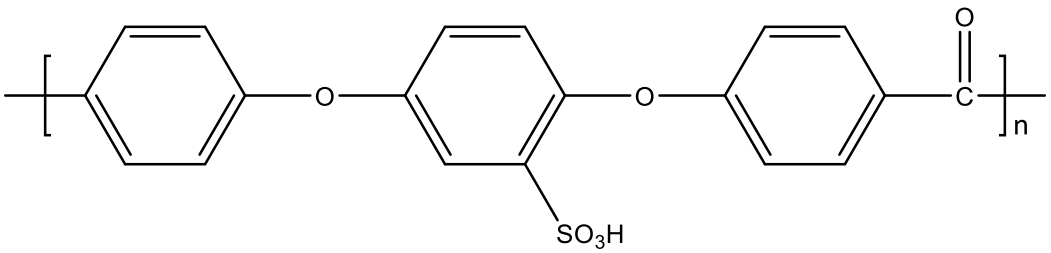

Figure 2.5 Structure of sulfonated poly(ether ether ketone).

These materials are chosen because of their excellent ion conductivity, however, sulfonic acid and quaternary ammonium groups are not catalytically active, as can be seen from Table 2.1. That is why the IL will be modified with a catalyst. The catalysts chosen are branched polyethyleneimine (PEI) and polyacrylic acid (PAA), of which their structures are shown in Figure 2.6.

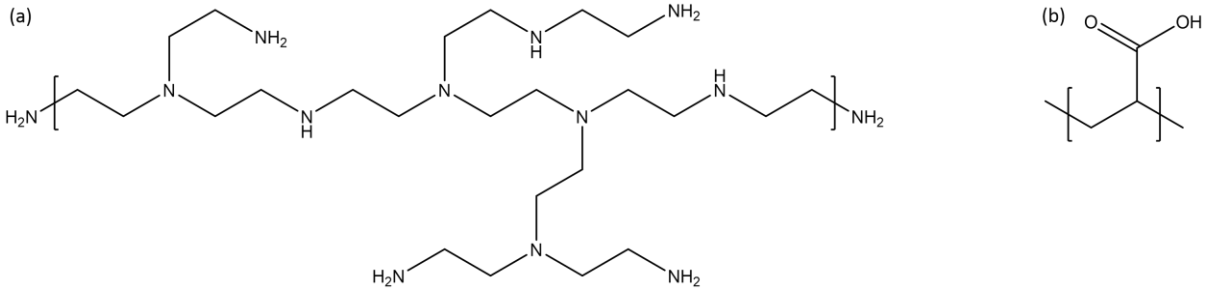

Figure 2.6 Structures of (a) polyethyleneimine (PEI) and polyacrylic acid (PAA).

PEI and PAA are both weak polyelectrolytes (PEs) and possess a wide variety of functional groups that are catalytically active (see Table 2.1). Incorporation of PEI and PAA in the IL introduces a wide spectrum of pK_a values, so WD can be catalyzed via both the weak base and weak acid mechanism.[33] PEI and PAA will be introduced to the IL via the layer-by-layer (LbL) method, which will be discussed in detail in the following section.

2.4. Layer-by-layer technique

The LbL technique is often used in the membrane field as a facile, environmentally friendly and scalable technique to prepare nanofiltration membranes with highly tunable properties.[70–74] The LbL method is a technique where a charged surface is coated by the alternating adsorption of oppositely charged PEs.[75] PEs are polymers with functional groups that ionize in polar solvents, such as water. When a negatively charged surface is exposed to a positively charged PE, a polycation (PC), a monolayer of the PC adsorbs to the surface of that support. Charge overcompensation reverses the charge of the support and no more PC can adsorb. A new monolayer of a negatively charged PE, a polyanion (PA), can now readily adsorb to the surface. The set of one PC and one PA layer is called a bilayer. This process can successfully be repeated until the desired number of layers is achieved.[74,76] The PC and PA used in this work, PEI and PAA, will be adsorbed on electrospun SPEEK nanofibers. The build-up of such a polyelectrolyte multilayer (PEM) on a SPEEK nanofiber is schematically shown in Figure 2.7.

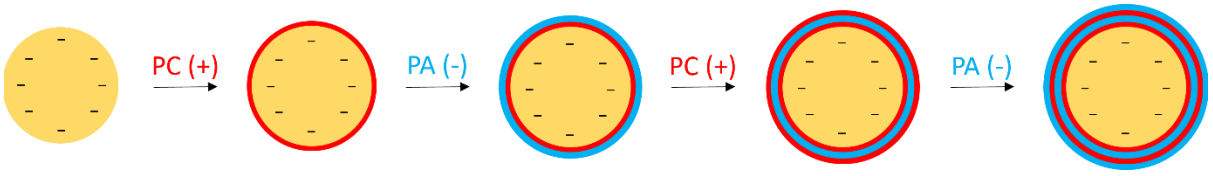

Figure 2.7 Schematic representation of the build-up of a polyelectrolyte multilayer by alternating adsorption of a polycation and a polyanion on a negatively charged SPEEK fiber.

The LbL method thrives in its simplicity and versatility. The practical setup can be as simple as manually dipping the support in beakers filled with the PE solutions. Any excess PE is simply removed by washing the support after each adsorption step. The adsorption step typically lasts between one minute and one hour, but it has been demonstrated that agitation of the solution bath can significantly reduce the time it takes to form a layer.[75,77] Because it is such an easy procedure, it can also be easily automated. Rapid layering of large, planar supports can be achieved in a roll-to-roll process, which has the added benefit of being easily scalable to industrial proportions.[78,79] The biggest advantage of the LbL method, however, is the precise control of the PEM properties by varying the number of layers and coating conditions. Factors such as pH, salt concentration, type of salt, PE type and concentration all influence the PEM growth.[43,71–73,80] To understand how these factors influence the PEM growth a better understanding of the mechanism behind PE adsorption is needed.

2.4.1. Layer-by-layer adsorption mechanism

Pioneers in the LbL research field came to the conclusion that the driving force behind PEM growth was the ionic attraction between oppositely charged PE segments.[81,82] However, if the adsorption was driven by Coulombic forces an exotherm would be expected upon association. Multiple studies have shown that the generated heat upon complexation is only a few kJ mol^{-1}, leading to the conclusion that association is entropic in nature.[83,84] It is now widely accepted that the gain in entropy caused by the release of counter-ions upon assembly is the main driving force for PEM growth.[73,76,83–85] The charged segments associate with a 1:1 stoichiometry, enforcing the counterions into solution. This is schematically shown in Figure 2.8, with Na^+ and Cl^- as counter-cation and -anion, respectively. It is exactly this mechanism what gives the LbL method its versatility. The PEM growth is controlled by the magnitude of the entropic gain, which in turn can be controlled by the background salt concentration (ionic strength) of the coating solutions.

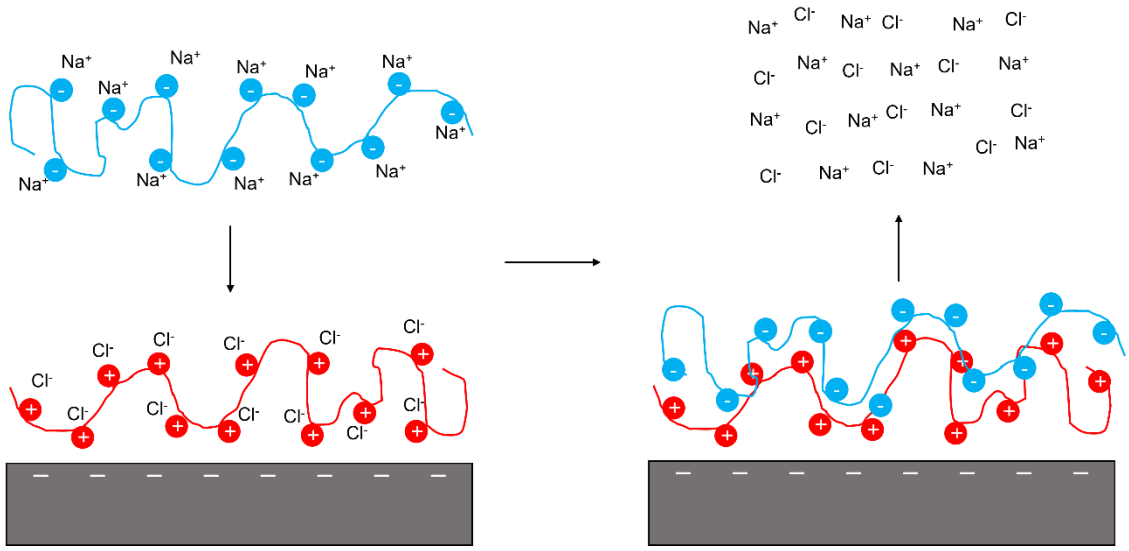

Figure 2.8 Schematic representation polyelectrolyte adsorption driven by the release of counter-ions.

Each charged PE segment can be seen as an adsorption site for an oppositely charged PE segment. At low ionic strength, the release of counter-ions results in a large entropy gain, as the salt concentration increases significantly. The charges on the PEs are then balanced by the charges of the oppositely charged PE. This type of compensation is called "intrinsic charge compensation". At higher ionic strengths, the gain in entropy is reduced compared to that at lower ionic strengths, as there is a high amount of salt ions in solution. As a result, the counter-ions are inclined to remain bound to the PE. The charges of the PE are then compensated by the counter-ions. This type of compensation is called "extrinsic charge compensation". The relation between intrinsically and extrinsically compensated PE segments is described by Eq. 2.10.[80]

$$Pol^{-}Pol^{+}_{PEM} + M^{+}_{aq} + A^{-}_{aq} \rightleftharpoons Pol^{-}M^{+}_{PEM} + Pol^{+}A^{-}_{PEM} \qquad \text{Eq. 2.10}$$

Here, Pol^{-} and Pol^{+} denote PA and PC segments, respectively. M^{+} are counter-cations and A^{-} are counter-anions. The subscript *PEM* denotes a PE segment that is part of the multilayer and the subscript *aq* denotes PE segments or counter-ions that are free in solution. At the left hand side of Eq. 2.10, the PEs are intrinsically compensated within the PEM, with the counter-ions free in solution. From this equilibrium it can readily be seen how the ionic strength influences the type compensation that occurs. At higher background salt concentrations, the equilibrium shifts to the right and the PEs are more extrinsically compensated. The type of compensation has a large influence on the structure of the PEs and therefore also on the final PEM structure.

Without salt or at very low ionic strengths, because of intrinsic charge compensation, the PE chains are oriented flat and parallel to the support surface.[86,87] At higher ionic strengths, because of extrinsic charge compensation, the salt ions in solution tend to screen the fixed charges on the PE. This causes the chains to take on a coiled conformation and reduces the amount of available adsorption sites.[88] Because there are less adsorption sites available, more PE needs to adsorb for surface charge reversal to occur. The coiled chain conformation also allows more PE to adsorb per unit area. These effects result in thicker, but also more open PE layers.[72] The effects of intrinsic and extrinsic charge compensation are schematically depicted in Figure 2.9a and Figure 2.9b, respectively, and show how the ionic strength of the coating solution can affect PEM growth.

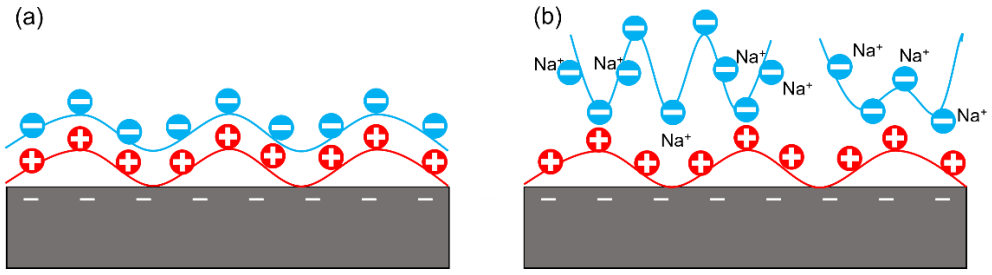

Figure 2.9 Schematic representation of the effect of (a) intrinsic and (b) extrinsic charge compensation on the polyelectrolyte layer growth.

Besides the ionic strength, there are other factors, *e.g.* charge density and ionization degree, influencing the PE chain structure and thus the PEM growth. Here the charge density is defined as the number of charged monomer units per PE chain. PE chains with high charges densities tend to elongate due to mutual repulsion of the charged PE segments, resulting in flat, dense layers upon association.[89] PE chains with lower charge densities tend to form coils and, just like extrinsically charge compensated PEs, form thicker PEMs. Similar to the charge density, the degree of ionization of a PE chain also influences PEM growth.[85,90] Strong PEs are completely ionized in water, but for weak PEs

the degree of ionization becomes a function of the pH of the coating solution.[85,90] The degree of ionization in weak PEs essentially determines the charge density of the PE and can control the PEM growth in a similar way as the ionic strength of the coating solution does. For example, a weak polyacid is completely ionized when it is brought into a solution with a high pH. In case of a high charge density PE, the chains are elongated and form thin layers (Figure 2.10a). As the pH decreases, the ionization degree and therefore the charge density decrease as well. This causes PE chains to adopt more coiled structures and results in thicker PEMs (Figure 2.10b).

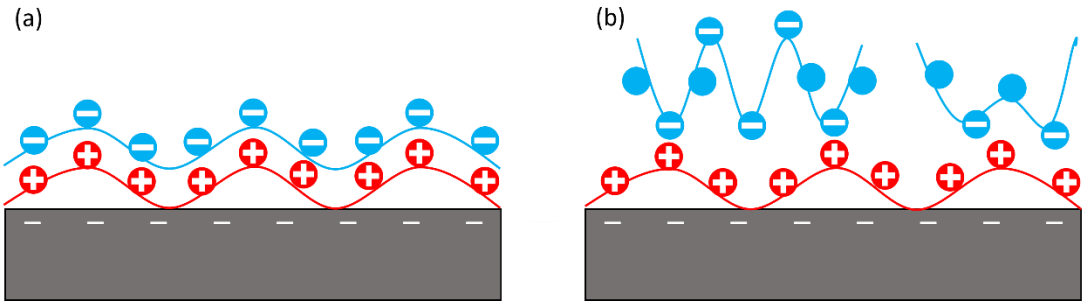

Figure 2.10 Schematic representation of polyelectrolyte adsorption of a weak polyanion at (a) a high ionization degree and (b) a low ionization degree.

The PEs used in this study, PEI and PAA, are both weak PEs. The ionic strength and pH of the coating solutions can therefore be used to control the PEM growth and tune the final structure of the PEI and PAA multilayers. The branched PEI chains contain primary, secondary and tertiary ammonium groups, which all show favourable catalytic activity towards WD (Table 2.1). The PAA chains, containing carboxylic acid groups, are even more catalytically active. By using both PEI and PAA, a broad range of pK_a values are present, allowing the WD reaction to be enhanced via both the weak acid and weak base reaction mechanism. PEI and PAA multilayers are deposited onto electrospun SPEEK nanofibers. Combining the LbL method with electrospinning allows for the deposition of a thin catalyst layer with a high active site density across a large surface area, while simultaneously enhancing WD and the mechanical properties by gaining a 3D electrospun bipolar junction.

The objective of this study therefore is to systematically investigate the influence of both ionic strength and pH on PEI and PAA multilayer growth. The PEM growth will be monitored via fixed angle optical reflectometry on a model surface. The CEL and AEL will be prepared via wire-electrospinning, from SPEEK and FAA-3, respectively. Electrospun SPEEK nanofibers will be coated with PEI and PAA multilayers via the dip coating method. The LbL modified SPEEK mats are sandwiched between pristine SPEEK and FAA-3 mats and are then densified via hot pressing. The catalytic effects of PEI and PAA on WD will be assessed electrochemically, by recording polarization curves and measuring the permselectivity of the acquired BPMs.

Chapter 3. Experimental

This chapter contains the materials and methods used to fabricate and characterize LbL modified electrospun BPMs. The methods section will be divided into three parts. The first part will describe a study on the influence of external factors controlling PEM growth, the second part will describe the fabrication procedure of the BPMs and the third part will describe the (electrochemical) characterization of the LbL modified electrospun BPMs.

3.1. Materials

Fumion® E-500, Sulfonated poly(ether ether ketone) (SPEEK), with an IEC of around 2.0 meq/g (cation-exchange polymer) and Fumion FAA-3 with an IEC of 2.5-3.0 meq/g (anion-exchange polymer) were purchased from FumaTech-BWT GmbH (Germany). The two polyelectrolytes, branched polyethyleneimine (PEI, M_n = 60 kDa, M_w = 750 kDa, 50 wt% in water), poly(acrylic acid) (PAA, Mw = 100 kDa, 35wt% in water), 1M hydrochloric acid (HCl, Supelco®), 1M sodium hydroxide (NaOH, Supelco®) and N,N-Dimethylacetamide (>99%) were obtained from Sigma Aldrich (The Netherlands). Sodium sulfate decahydrate ($Na_2SO_4 \cdot 10H_2O$) (M_w = 322.20 g/mol) was purchased from ThermoFisher Scientific (The Netherlands). Sodium chloride (NaCl) (M_w = 58.44 g/mol) pharmaceutical grade (Sanal® P) was kindly supplied by Nouryon (the Netherlands). All solutions were prepared with ultrapure water PURELAB Option, Veolia Water Solutions & Technologies (the Netherlands). All chemicals were used as received.

3.2. Polyelectrolyte multilayer growth

Optical fixed angle reflectometry was used to study the influence of PE concentration, background salt concentration and pH on the growth of PEI and PAA multilayers on a flat model surface. Coating solutions of 0.01 and 0.1 wt% PEI and PAA were prepared at ionic strengths varying from 5 to 500 mM NaCl. The pH of the solutions was varied between 4 and 10 and was adjusted by adding appropriate amounts of 1M HCl or NaOH. Rinsing solutions, called “solvent”, were prepared at the same ionic strength and pH as the coating solutions, but without addition of PE.

A silicon wafer was thermally treated for 1 hour at 1000°C until an SiO_2 top layer was formed. The wafer was cut into 1 cm wide strips, with SiO_2 layers ranging from 65 to 85 nm, as determined by ellipsometry. Each strip was cleaned in a UV/ozone reactor for 5 minutes prior to each experiment. The wafer was placed in a stagnation point flow cell and the cell was filled with solvent. The wafer was hit with polarized, monochromatic light (He-Ne laser, 632.8 nm) around the Brewster angle (71°). The light was reflected towards the detector, where it was split into its p- and s-polarized components. The output signal of the reflectometer (*S*) is defined as the ratio between the intensities of the reflected components according to Eq. 3.1:

$$S = \frac{I_p}{I_s} \qquad \text{Eq. 3.1}$$

Here, I_p and I_s are the intensities of the parallel and perpendicular components, respectively. Alternating layers of PEI and PAA were adsorbed onto the wafer by successively exposing the wafer to the PEI and PAA coating solutions for 5 minutes using a custom-built valve system (Wageningen University & Research, The Netherlands). Because the SiO_2 layer is negatively charged in water, the wafer was exposed to the polycation (PEI) solution first, for 5 min, followed by a rinsing step with only solvent. The wafer was then exposed to the polyanion (PAA) solution for 5 min, again followed by a rinsing step of 5 min with only solvent. This process was repeated until 6 bilayers were formed. The buildup of bilayers of PEI and PAA on a silicon wafer is depicted in Figure 3.1. Each coating step was

followed by a rinsing step, where the wafer was flushed with solvent for 5 minutes. This procedure was repeated until the desired amount of bilayers was deposited. The use of a stagnation point flow cell ensures that PE transport at the measuring spot on the wafer was purely diffusion-based.[91]

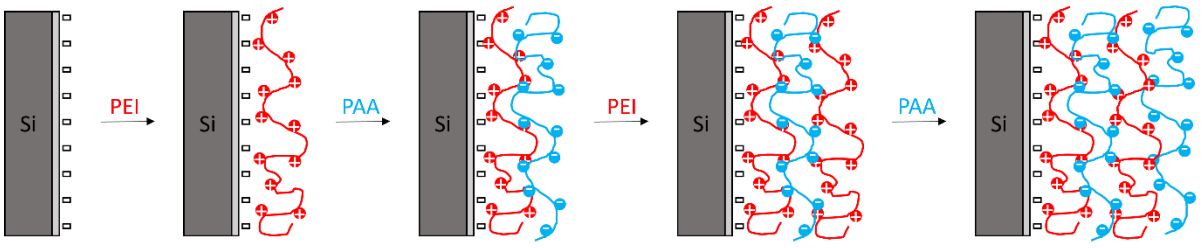

Figure 3.1 Schematic representation of the buildup of bilayers of PEI and PAA on a silicon wafer with a SiO_2 layer (in light grey) during reflectometry experiments.

The change in signal (ΔS) caused by the adsorption of PEI and PAA is directly proportional to the amount of adsorbed mass onto the wafer, according to Eq. 3.2.

$$\Gamma = \frac{\Delta S}{S_0} Q \qquad \text{Eq. 3.2}$$

In this equation, Γ is the amount of adsorbed mass on the wafer in mg m^{-2}. S_0 is the starting output signal of the bare silicon wafer (-). The sensitivity factor, Q (mg m^{-2}), is dependent on the following factors: the angle of incidence of the laser (θ), the refractive indices (n) of the PEs, the thicknesses (d) of the layers on the wafer (including the SiO_2 layer) and the refractive index increment (dn/dc) of the adsorbate. The silicon wafer was alternatingly exposed to the PE solutions by a custom built valve setup..

The Q factor was determined in the Prof. Huygens software using the following values: θ = 70°C, $n_{silicon}$ = (3.85, 0.02), n_{silica} = 1.46, d_{silica} = 79.4 nm, $(dn/dc)_{PEI}$ = 0.108 L kg^{-1}, $(dn/dc)_{PAA}$ = 0.16 L kg^{-1}. Because of the differences in dn/dc for PEI and PAA, different Q factors were determined for both polymers. The Q factor for PEI was determined from the first adsorption step and the Q factor for PAA was determined from the second adsorption step. These same Q factors were then used for the determination of Γ for the remaining bilayers. For each reflectometry experiment, new Q factors were determined. Using reflectometry, the multilayer formation could be monitored in-situ and provided an indication of the amount of PE adsorbed as a catalyst layer in the electrospun SPEEK mats.

3.3. Membrane fabrication

The fabrication method of the LbL modified BPMs was a multi-step process. The CEL and AEL were produced from electrospun SPEEK and FAA-3 nanofiber mats, respectively. Based on the reflectometry results, PEI and PAA multilayers were deposited onto a SPEEK nanofiber sheet via the dip coating method. The LbL coated SPEEK sheet was sandwiched between multiple SPEEK and FAA-3 sheets and the stack was hot pressed into a dense BPM.

3.3.1. Electrospinning

Electrospinning was carried out on a Nanospider NS LAB, Elmarco, Czech Republic wire-electrospinner. The temperature and relative humidity (RH) of the electrospinning chamber were controlled using a desiccant dehumidifier system (ML270PLUS, Munters, The Netherlands). SPEEK and FAA-3 nanofiber mats were prepared by electrospinning dope solutions of 20 and 26 wt%, respectively. The 20 wt% SPEEK solution was prepared by dissolving 13 g of dried SPEEK fiber in 52 g of dry DMAc. The 26 wt%

FAA-3 solution was prepared by dissolving 13 g of dried, shredded FAA-3 film in 37 g of dry DMAc. Both solutions were left on a roller bench overnight under argon atmosphere.

SPEEK was used to fabricate the CEL and FAA-3 was used for the AEL. All electrospinning parameters are summarized in Table 3.1. The total electrospinning time varied for each batch and depended on the amount of solution available. The carrier had to be refilled several times during the electrospinning process.

Table 3.1 Electrospinning parameters used for the production of SPEEK and FAA-3 nanofibers.

CEL		**AEL**
	Polymer solution	
SPEEK	Polymer	FAA-3
DMAc	Solvent	DMAc
20 wt%	Concentration	26 wt%
	Electrospinning	
4.1 g kg^{-1} (25%)	Relative humidity	3.2 g kg^{-1} (20%)
22°C	Temperature	22°C
100 mm s^{-1}	Carrier speed	100 mm s^{-1}
0.8 mm	Aperture	0.8 mm
80 kV	Voltage	80 kV
15 cm	Working distance	24 cm
5 mm min^{-1}	Substrate speed	5 mm min^{-1}

3.3.2. Layer-by-layer assembly of polyelectrolyte catalyst layers

Electrospun SPEEK was chosen as the substrate for the LbL deposition of PEI and PAA multilayers. The conditions used for the coating solutions were based on the optical reflectometry results. The dip coating procedure went as follows: an electrospun SPEEK sheet of 9.5 x 9.5 cm was cut out and clamped between two plastic spacers. PEI and PAA multilayers were grown on the SPEEK nanofibers by alternatingly submerging the sheet in PEI and PAA coating solutions for 15 minutes, while shaking gently at 50 rpm. Each coating step was followed by a rinsing step of 15 minutes in an NaCl solution of equal ionic strength and pH. The procedure is schematically shown in Figure 3.2. When the desired amount of bilayers was achieved, the LbL coated SPEEK sheet was rinsed a final time in deionized water for 15 minutes to remove any salt that may have accumulated. It was then transferred to a vacuum oven to dry overnight at 60°C.

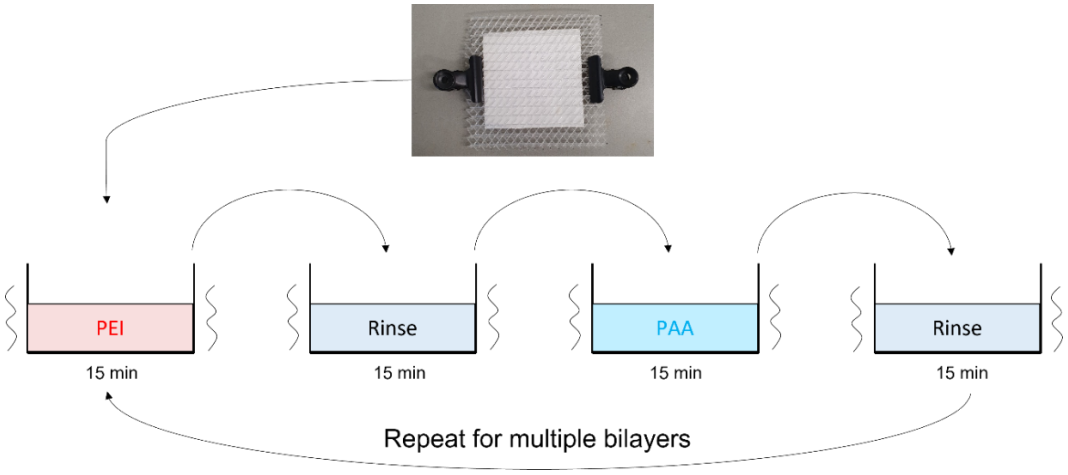

Figure 3.2 Schematic overview of the dip coating procedure used for the growth of PEI and PAA multilayers on an electrospun SPEEK sheet.

3.3.3. Densification with hot pressing

The LbL coated SPEEK sheet had shrunk down to roughly 8 x 8 cm after drying. Therefore, several pristine electrospun SPEEK and FAA-3 sheets were cut out of 8 x 8 cm until the combined thickness of the SPEEK sheets matched that of the combined FAA-3 sheets. The LbL coated SPEEK sheet was sandwiched between the pristine SPEEK and FAA-3 sheets, as shown in Figure 3.3. The stack was then placed between two Teflon sheets and transferred to a Fontijne LabEco hot pressing machine to be hot pressed at 150°C and 100 kN (156 bar) for 30 – 60 min. The temperature of 150°C was chosen because it is close to the glass transition temperature of SPEEK and FAA-3 (151 and 160°C, respectively). The densified BPMs were submerged in a 0.5 M NaCl solution for conditioning.

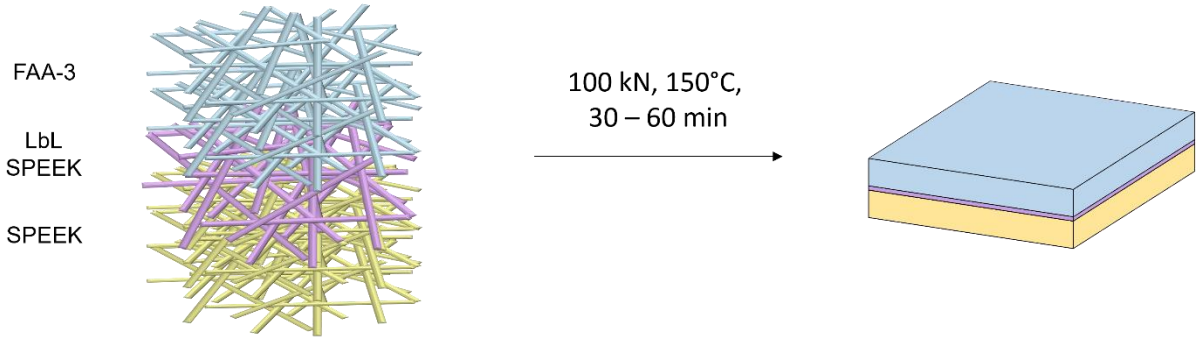

Figure 3.3 Schematic representation of the LbL coated SPEEK sheet (purple) sandwiched between multiple pristine SPEEK (yellow) and FAA-3 (blue) sheets before and after hot pressing at 100 kN and 150°C for 30 to 60 minutes.

3.4. Membrane characterization

3.4.1. Scanning electron microscopy and energy dispersive X-ray spectroscopy

The morphology of the electrospun, nanofiber mats as well as the hot pressed BPMs was characterized by scanning electron microscopy (SEM), using a JEOL JSM-IT100 equipped with EDS. The samples were cryogenically fractured in liquid nitrogen to obtain cross-sectional images. Elemental mapping of the BPM cross-sections was performed with energy dispersive X-ray spectroscopy (EDS). To prevent charging, all samples were coated with platinum for 60s at 40 mA using a JEOL JFC-2300 HR sputter coater.

3.4.2. Electrochemical characterization

One of the most important properties of BPMs is their performance in an electrochemical cell. The characteristics explored in this work are the permselectivity and the polarization behavior of the fabricated BPMs.

3.4.2.1. Permselectivity

The permselectivity of a BPM is determined by taking the ratio between the measured experimental and the theoretical open circuit voltage (OCV). The theoretical OCV is calculated using the Nernst equation (Eq. 3.3).

$$E_{tot} = E_{acid} + E_{base} = \frac{RT}{zF}\ln\left(\frac{\alpha[H^+]_{acid}}{[H^+]_{junction}}\right) + \frac{RT}{zF}\ln\left(\frac{[OH^-]_{junction}}{\alpha'[OH^-]_{base}}\right) \qquad \text{Eq. 3.3}$$

In this equation, E is the potential in V, R is the universal gas constant (8.3145 J mol^{-1} K^{-1}), T is the absolute temperature in K, z is the valency of the ions and F is the Faraday constant (96 485 C mol^{-1}). $[H^+]$ and $[OH^-]$ are the molar H^+ and OH^- concentrations and α and α' their respective activity coefficients. Using Eq. 3.3, the theoretical OCV was calculated to be 0.775 V. To measure the OCV of the fabricated BPMs, the BPM was placed in between a 0.5 M HCl and 0.5 M NaOH solution. The BPM was positioned in such a way that the CEL was facing the acid compartment and the AEL was facing the base compartment, as can be seen in Figure 3.4. The OCV of all membranes was measured for 1 hr in duplicate or triplicate. The permselectivity of the fabricated BPMs was compared to that of a commercial one (Fumasep® FBM-PK, Fumatech GmbH, Germany).

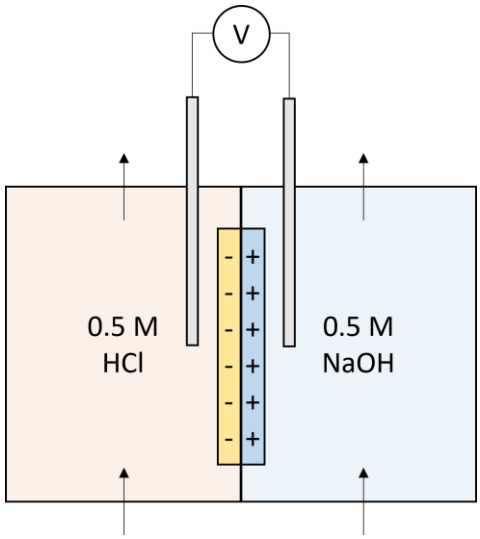

Figure 3.4 Permselectivity setup.

3.4.2.2. Polarization behavior

Polarization curves were recorded using a custom made six-compartment cell. Each compartment was separated by either a CEM or an AEM in the configuration as shown in Figure 3.5. The two outer compartments contained an electrode rinse solution consisting of 0.5 M Na_2SO_4. The measuring compartments in the middle, adjacent to the BPM, contained a 0.5 M NaCl solution. The compartments in between the monopolar membranes (second and fifth) also contained a 0.5 M NaCl buffer solution, to reduce the influence of the electrode reactions at the working electrodes. All solutions were kept at a constant temperature of 25°C using a water bath and are recirculated through their respective compartments with a flow rate of 170 mL min^{-1}. Prior to each measurement, the BPMs were soaked in 0.5 M NaCl for at least 24 h for conditioning. The BPMs were placed in a Teflon holder

with two circular holes, leaving an active membrane area of 17.35 cm^2. A current was driven through the cell by performing the oxygen evolution reaction (OER, Eq. 3.4) at the anode and the hydrogen evolution reaction (HER, Eq. 3.5) at the cathode.

Anode $$2\,H_2O \rightarrow O_2 + 4\,H^+ + 4\,e^-$$ Eq. 3.4

Cathode $$2\,H^+ + 2\,e^- \longrightarrow H_2$$ Eq. 3.5

The potential drop across the BPM was measured with Ag/AgCl reference electrodes, placed in Haber-Luggin capillaries close to the membrane. These are indicated by the grey bars in Figure 3.5.

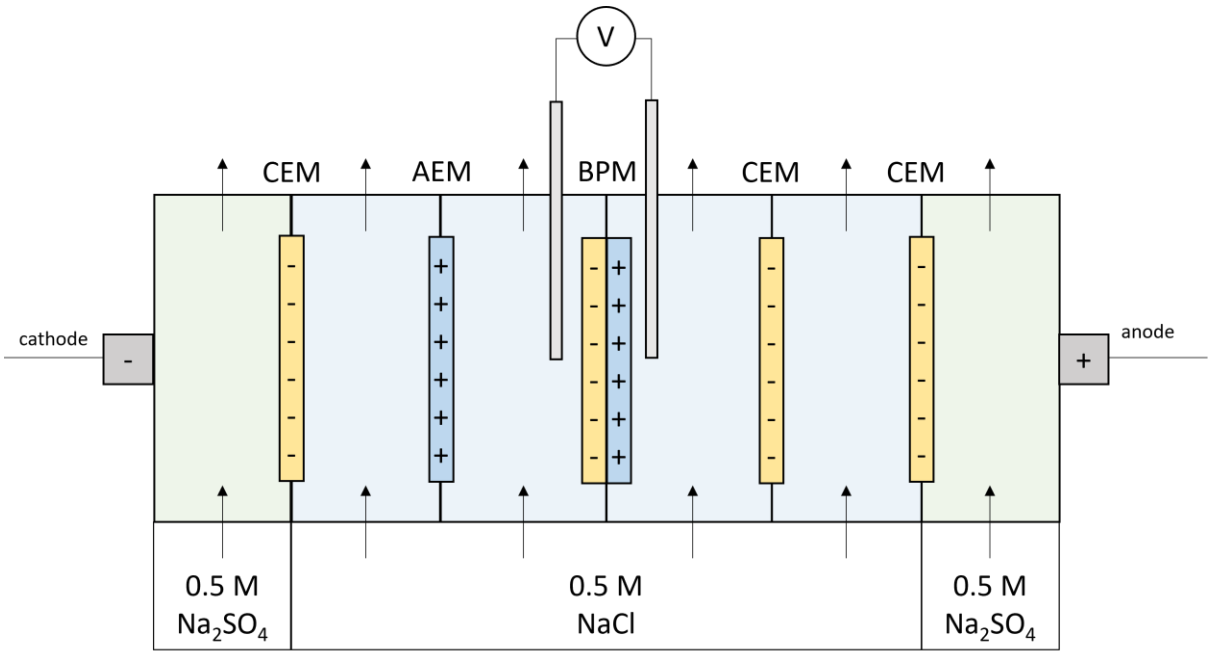

Figure 3.5 Six compartment cell used to record polarization curves of the fabricated bipolar membranes.

Current densities in the range of 0 – 10 mA cm^{-2} were applied for 120 s each, using a Ivium n-stat (IVIUM Technologies BV, The Netherlands), while measuring the potential across the BPM. Blank measurements were performed before and after the membrane measurements to correct for the potential drop caused by the electrolyte solution. The potential drop over the BPM was measured in triplicate. The resulting polarization curves were used to assess the WD performance of the fabricated BPMs by extracting the WD onset potential and the BPM resistance.

Chapter 4. Results and Discussion

In this chapter, the results of the previously described experiments will be discussed. The influence of PE concentration, ionic strength and pH on PEI and PAA multilayer growth was assessed on a silicon wafer with optical fixed angle reflectometry. With the acquired knowledge, BPMs were prepared from electrospun SPEEK and FAA-3, where SPEEK was modified with the LbL dip coating technique. The obtained sheets were then combined and hot pressed into dense BPMs. The morphology of the electrospun materials, the LbL coated SPEEK and the densified BPMs was characterized by SEM and EDS. The electrochemical performance of the BPMs was assessed by recording polarization curves and by measuring the permselectivity.

4.1. Polyelectrolyte multilayer growth

Since it was not possible to monitor PEI and PAA adsorption on the SPEEK nanofibers directly, optical fixed angle reflectometry was used as an in-situ method to monitor PEM growth on a model surface. The PEI/PAA multilayer growth was followed by alternatingly exposing a silicon wafer with a SiO_2 top layer to solutions of PEI and PAA and measuring the difference in signal upon adsorption. The effect of the PE concentration and ionic strength of the solution was determined by using PEI and PAA solutions at concentrations of 0.01 and 0.1 wt% and at ionic strengths varying between 5 and 500 mM NaCl. The pH of the solutions was varied between 4 and 10. The ionic strength and pH of the PE free rinsing solutions (solvent) was identical to that of the coating solutions for all experiments but one. The pH of all solutions was left unadjusted in that experiment.

A typical adsorption curve of the LbL buildup of a PEI and PAA multilayer, as measured with reflectometry, is shown in Figure 4.1. The difference in signal due to PEI and PAA adsorption ($S - S_0$) is plotted as a function of time. At the start of the experiment, the wafer was rinsed with solvent (s) to record a value for S_0. The PEM consists of six bilayers and is built up by alternatingly flushing a silicon wafer with a 0.01 wt% PEI (+) and PAA (-) solution at an ionic strength of 50 mM NaCl and at a pH of 6.5 for five minutes. Each coating step was followed by a rinsing step (s) to prevent complexation of PEI and PAA in bulk or inside the tubing and to wash away any excess or loosely bound PE.

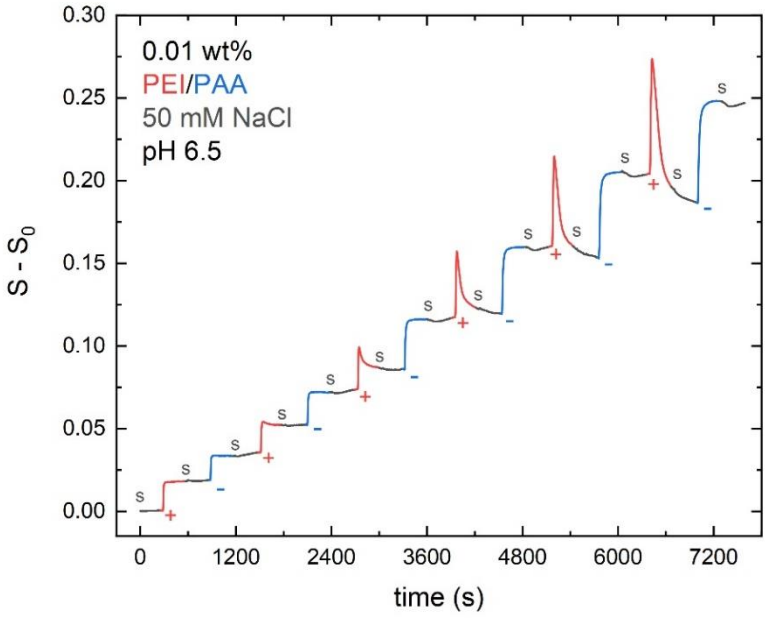

Figure 4.1 Example of a typical reflectometry experiment for PEI and PAA adsorption, where 's' = solvent '+' = PEI, '-' = PAA, $M_{w,\,PEI}$ = 750 kDa, $M_{w,\,PAA}$ = 100 kDa, $c_{PEI/PAA}$ = 0.01 wt%, [NaCl] = 50 mM, pH = 6.5.

The curve in Figure 4.1 shows stepwise growth with an almost instantaneous signal increase upon PE adsorption. In the first adsorption step the signal plateaus and stabilizes quickly, indicating no further PEI adsorption. The subsequent adsorption of PAA shows that the wafer is saturated with PEI and that its surface charge is reversed. The formation of the second bilayer follows a similar trend, but the adsorption behavior changes from the third bilayer and onward. A peak is observed in the PEI adsorption step, indicating that PEI adsorption is immediately followed by desorption. The size of these peaks grows larger for each subsequent bilayer. In the fifth and sixth bilayer the peak ends at a lower value than where it started, suggesting complete desorption of the PEI layer. However, the signal is observed to increase during each PAA step, indicating adsorption. PAA only adsorbs when the surface is positively charged, suggesting the adsorbed PEI layer is still present at the PEM surface.

Kovacevic et al. proposed a convincing explanation for these observed "overshoots." The researchers stated that, similar to polymers, a PEM exists in a "glassy" state at low ionic strength and in a "liquid" state at higher ionic strengths.[92] Above a critical salt concentration (c_{cr}) the PEM dissolves completely due to screening of the ionic charges on the PEs. Below c_{cr} there is a two phase system with a dense PEM phase and a dilute PEI or PAA solution phase. At high concentrations of PEI or PAA, positively or negatively charged soluble PE complexes can be formed, respectively. When the PEM is in the liquid state and is flushed with PEI solution, at first a monolayer adsorbs to the surface, causing the signal to increase. After saturation, PEI mixes with the previously deposited PAA layer. This allows PAA to reach the boundary with the dilute solution. When an excess of PEI is supplied, soluble coacervate complexes (SCC) can be formed between PEI from the solution and PAA within the PEM. This causes the multilayer to erode and thus the signal to decrease. The reason that, under these conditions, this behavior is only seen during PEI adsorption and not with PAA probably is correlated with the mobility and interdiffusion of PEI.[92] The PEI monomer is highly branched and contain primary ammonium groups, which bind strongly to the PEM. The carboxylates on PAA are weakly associated with the PEM and are therefore more susceptible to form SCCs with PEI in solution.[93] The reason for the "overshoots" to only occur after a certain number of bilayers is that chains that are close to the surface are immobilized because they have stronger interactions with the surface's charges.[94]

Another explanation is given by Wågberg et al.[95] They reasoned that these overshoots are not caused by desorption, but rather by a change in the optical properties due to rearrangement of the PEs in the PEM. In reality it is more likely to be a combination of both processes. While the exact origin of the overshoot peaks is still in debate, these data show that the PEI and PAA couple is suitable for the LbL formation of PEMs, since an increase in overall adsorption is observed when adding more bilayers. The following section will discuss in further detail how the ionic strength and PE concentration affects the PEM growth.

4.1.1. Influence of ionic strength and PE concentration

The influence of ionic strength and PE concentration on the total adsorbed amount of PE as a function of the number of bilayers is shown in Figure 4.2. The values of ΔS at the end of each solvent step were used to calculate the adsorbed mass using Eq. 3.2. The raw reflectometry signals are shown in Figure A-1 in the Appendix A. Figure 4.2a shows the effect of ionic strength on the total adsorbed mass at PE concentrations of 0.01 wt% and at a pH of 6.5. This pH was chosen here because both PEI and PAA are almost completely ionized at pH 6.5. Linear PEM growth is observed at the lower salt concentrations (5 and 50 mM). This is because at low ionic strengths, PE charges are predominantly intrinsically compensated, resulting in a thin, dense PEM.[71] As the ionic strength increases from 50 to 500 mM NaCl, the adsorption behavior changes drastically and the effect of extrinsic charge compensation is

clearly shown. The PE charges are shielded by the salt ions in solution, causing the PE chains to adopt a more open and coiled conformation. Because of the reduced amount of available binding sites, more PE is required to adsorb per adsorption step before charge overcompensation occurs and the surface charge is reversed. The total adsorption therefore reaches much higher values at 500 mM NaCl than at 5 and 50 mM NaCl. The adsorption per bilayer at 500 mM NaCl seems to increase per step, indicating exponential growth of the PEM. Exponential growth is believed to be caused by interdiffusion of PEs into the multilayer and increases as the ionic strength of the coating solution increases.[73]

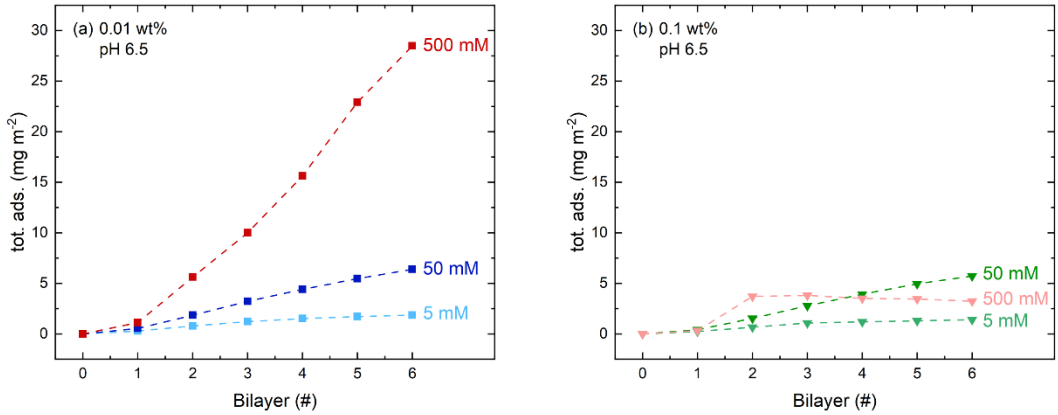

Figure 4.2 Total adsorbed amount of PEI and PAA as a function of the number of bilayers at a pH of 6.5 and ionic strengths of 5, 50 and 500 mM NaCl and polyelectrolyte concentrations of (a) 0.01 wt% and (b) 0.1 wt%.

Figure 4.2b shows the influence of ionic strength on the PEM growth at a pH of 6.5 and PE concentrations of 0.1 wt%. The increase of the PE concentration does not seem to affect the total adsorbed mass for 5 and 50 mM NaCl. This is because reversal of the surface charge prevents further adsorption, making the process self-terminating and independent of PE concentration. However, at 500 mM there is an initial increase in adsorption from one to two bilayers, but from there, the total adsorption seems to plateau and even decreases as more bilayers are added. This desorption is most likely caused by the formation of SCCs, similar to the decrease in signal as explained for Figure 4.1. Because of the higher PE concentration, there is an even higher excess of PC in the PEI adsorption step. This allows for more positively charged SCCs to be in solution. The combination of loosely bound PE chains in the PEM due to extrinsic charge compensation at 500 mM and the excess of PEI in solution prevents PEM growth. Apparently, up to two bilayers the PEM exists in the glassy state, while the rest of the PEs dissolve and are washed away. These results indicate that it is not possible to build a PEM of more than two bilayers at PE concentrations of 0.1 wt% and at an ionic strength of 500 mM NaCl at a pH of 6.5. For this reason, the following experiments are all carried out at PE concentrations of 0.01 wt%.

4.1.2. Influence of pH

Since PEI and PAA are weak polyelectrolytes, their ionization degree (α) is dependent on the pH of the coating solutions. Therefore, similar to the ionic strength, the pH of the coating solutions can be used to control the PEM growth behavior. Coating solutions were prepared of 0.01 wt% PEI and PAA at an ionic strength of 50 mM NaCl. The pH was varied between 4 and 10. In all cases, the pH of the rinsing solutions was identical to the coating solutions, except for one. The pH of all solutions was left unadjusted for that experiment. The respective pH values of the PEI, PAA and rinsing solution were 10, 3.7 and 5.8. The α of PEI and PAA as a function of pH were determined via zeta potential

measurements (method not discussed in this report) and the results are shown in **Error! Reference s ource not found.**. The α of PEI and PAA at the pH values used in reflectometry experiments are extracted from this graph and are summarized in Table 4.1.

Table 4.1 Degree of dissociation (α) of PEI and PAA at different pH values.

	Degree of ionization (α)	
pH (PEI/PAA)	**PEI**	**PAA**
10/3.7	40%	35%
4/4	90%	40%
6.5/6.5	90%	85%
8/8	40%	80%
10/10	40 %	95%

The total adsorption as a function of the number of deposited bilayers under these conditions is plotted in Figure 4.3. The reflectometry signals are shown in Figure A-3 in.

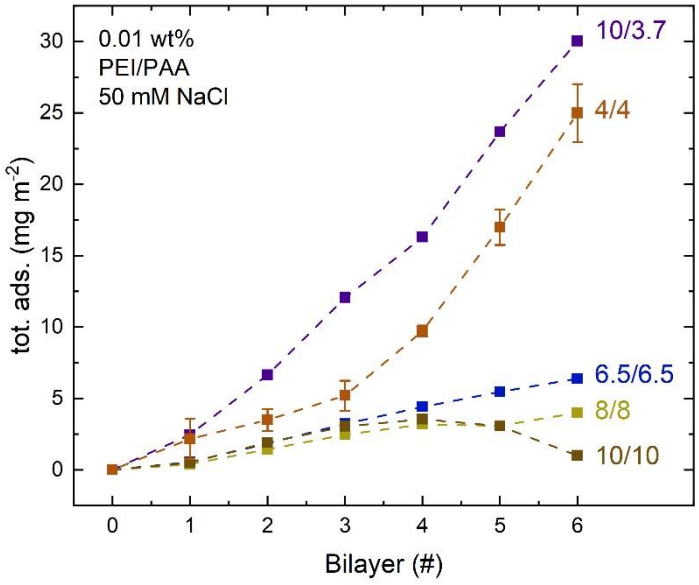

Figure 4.3 Total adsorbed amount of PEI and PAA as a function of the number of bilayers at 0.01 wt%, 50 mM NaCl and pH 4 – 10. For no pH adj., pH_{PEI} = 10, pH_{PAA} = 3.7, $pH_{solvent}$ = 5.8.

Figure 4.3 shows the total adsorbed amount of PE as a function of the number of deposited bilayers. The numbers next to the adsorption curves denote the pH of the respective coating solution, with the first number being the pH of the PEI solution and the second being the pH of the PAA solution. From Figure 4.3, it becomes evident that the PEI and PAA multilayer growth is strongly dependent on pH. At pH 10/3.7 the total adsorption seems to increase slightly exponentially. At pH 4/4 the total adsorption increases linearly for the first three bilayers and then also starts to grow exponentially. The total adsorption increases linearly for pH 6.5/6.5 and pH 8/8. At pH 10/10, the total adsorption increases linearly up to four bilayers and then decreases in the last two adsorption steps. Exponential PEM growth is believed to be caused by interdiffusion of either or both of the PEs into the existing multilayer.[96] The ability of a PE to diffuse through the PEM is dependent on the α, and therefore pH, of the PE. The diffusivity of both PEI and PAA becomes higher as α decreases.[85,97]

At pH 10/3.7, PEI and PAA have an α of 40% and 35%, respectively. Both PEs should be able to diffuse in and out of the multilayer at these pH values.[85,97] Looking at the PEM growth in Figure 4.3, this does seem to be the case, as the total adsorption increases exponentially per added bilayer. Then at pH 4/4, the α of PEI increases to 90%, while the α of PAA only increases to 40%. Even though PEI lost the ability to diffuse into and out of the multilayer, the PEM grows exponentially because of interdiffusion of PAA.[85] At pH 6.5/6.5 PEI and PAA both have a high α of 90% and 85%, respectively. At 50 mM NaCl both PEs adopt a linear conformation and have low diffusivity. Therefore, linear PEM growth is expected. This is confirmed by the adsorption curve in Figure 4.3. As the pH for both PEI and PAA goes up to 8/8, the α for PEI decreases to 40%, while the α for PAA remains high at 80%. Since the diffusivity of PEI should increase at lower α, exponential PEM growth was expected. However, linear growth is observed. Since PAA still has a high α, it might be that the elongated PAA chains prevent interdiffusion of PEI into the multilayer and linear PEM growth is maintained. The PEM growth at pH 10/10 looks similar to pH 8/8. The α for PEI remains at 40%, but the α of PAA increases to 95%. Again linear growth is observed as a function of the number of bilayers. However, after four bilayers the total adsorption starts to decrease. This decrease can be attributed to the increased hydrophilicity of PAA at higher pH, and thus high ionization degree, favoring the formation of these SCCs, resulting in a decrease in overall adsorption.[92]

From these results, it can be concluded that the pH of PAA is the predominant factor that determines the growth behavior of the PEI and PAA multilayer. There seems to be a trend between the α of PAA and the type of growth, as the growth transitions from linear to exponential with decreasing α. At high α values for PAA, the growth behavior seems to be independent of the α of PEI, as the growth regime remains linear even though the α of PEI changes. Then at low α for PAA and high α for PEI the growth becomes exponential because of diffusion of PAA into the PEM. Only when the diffusivity of PAA is high at low α, PEI is also able to diffuse into the multilayer at low α, reinforcing the multilayer growth. It is obvious that at pH 4/4 and 10/3.7 the most adsorption of PEI and PAA occurs and these conditions therefore are the most promising to use for the introduction of PEI and PAA into the BPM junction as a catalyst.

4.2. Morphological characterization

The BPM preparation method consisted of the following steps: 1) electrospinning of SPEEK and FAA-3 nanofiber mats, 2) deposition of PEI and PAA multilayers on a single SPEEK nanofiber mat using the LbL dip coating method, 3) hot pressing of the LbL modified SPEEK, sandwiched in between multiple pristine SPEEK and FAA-3 nanofiber sheets into a dense BPM. After each of these steps, the morphology of the obtained structures was characterized by SEM and EDS.

4.2.1. Morphology of nanofibers after electrospinning

SPEEK and FAA-3 nanofiber mats were electrospun from 20 and 26 wt% solutions in DMAc, respectively. The spinning parameters are shown in Table 3.1. Wire electrospinning is a roll-to-roll process and allows the production of nanofibers for hours on end, as long as a dope solution is supplied. In this work, the average spinning time was around one hour, yielding nanofiber mats of about a meter long and 30 cm wide. The morphology of the obtained mats was characterized with SEM. Figure 4.4 shows SEM images of the SPEEK and FAA-3 nanofibers at 500 and 5000 times magnification. It can be seen from Figure 4.4a that a largely homogeneous SPEEK nanofiber network is obtained, with an average fiber diameter of 138 ± 17 nm. Some thicker fibers and droplets are observed, however. The thickness of the nanofibers is, amongst others, dependent on the viscosity of the dope solution and increases with increasing viscosity.[98] Other factors affecting the fiber thickness are voltage, receiving distance, temperature and relative humidity.[99] Fluctuations in any of these

parameters may be the cause of the inhomogeneity of the fiber thickness. The droplets that can be seen in Figure 4.4a and the beadlike structures that are visible in Figure 4.4b are likely a consequence of insufficient solvent evaporation, resulting in wet fibers. As a consequence the polymer chains agglomerate and solidify.[100] As the wet fibers are no longer strained by the electric field, due to the surface tension of the solution, the chains shrink down into a hemisphere and droplets are formed. Figure 4.4c and Figure 4.4d show SEM images of the FAA-3 fiber structure at 500 and 5000 times magnification. Clear distinct fibers, with an average diameter of 361 ± 68 nm, are visible and only a few beads and droplets are found. The diameter of the FAA-3 fibers is significantly larger than that of the SPEEK fibers. This can be attributed to the higher concentration and, therefore, higher viscosity of the FAA-3 solution.

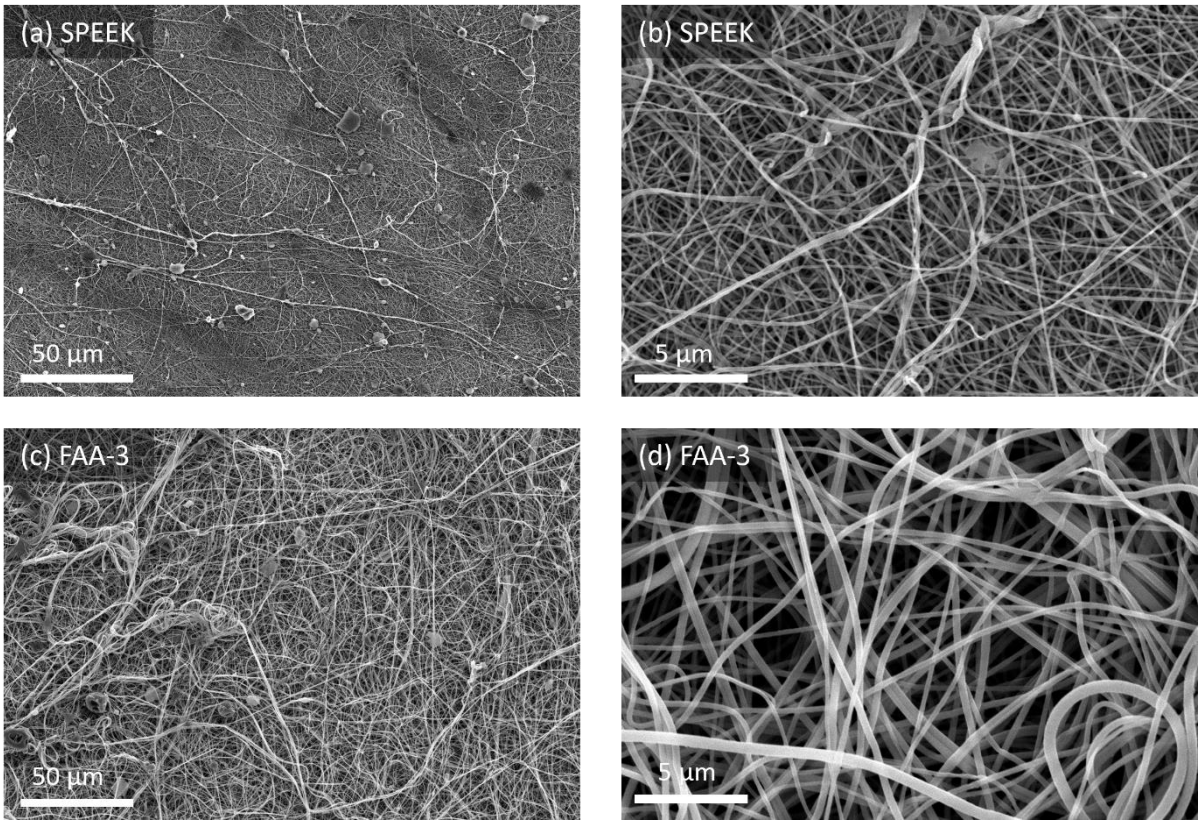

Figure 4.4 Scanning electron micrographs of electrospun SPEEK nanofibers at (a) 500 x and (b) 5000 x magnification and FAA-3 nanofibers at (c) 500 x and (d) 5000 x magnification.

4.2.2. Morphology of SPEEK nanofibers after LbL modification

To introduce the PE catalysts to the IL, PEI and PAA multilayers were deposited onto SPEEK nanofiber mats via the dip coating method. Only SPEEK mats were coated, because the FAA-3 mats lost their nanofiber structure after being submerged in water due to excessive swelling. The parameters that were varied during dip coating were: the number of bilayers, the weight concentration of the PEs, the ionic strength and the pH of the coating solutions. Figure 4.5 shows SEM images of SPEEK nanofiber that have been coated with 2 and 6 bilayers in solutions of 0.01 wt% PEI and PAA at a NaCl concentration of 50 mM and a pH of 6.5. Figure 4.5a shows the surface of the SPEEK fiber network after is has been coated with 2 bilayers of PEI and PAA. It shows a homogeneous fiber network, similar to that of uncoated SPEEK. From Figure 4.5b it can be seen that the fiber structure remained intact after the coating procedure. The fiber thickness seems to have increased slightly compared to the uncoated SPEEK fibers. During the coating procedure, the fibers take up water and swell. When the mats are dried at the end of the dip coating procedure, the fibers collapse into belts due to non-

uniform shrinkage.[101] This causes the fibers to flatten and appear thicker. However, distinct, individual fibers are still visible. This is a good indication that PEMs have actually formed around the SPEEK fibers and that they were not deposited as a film on the surface of the SPEEK mat.

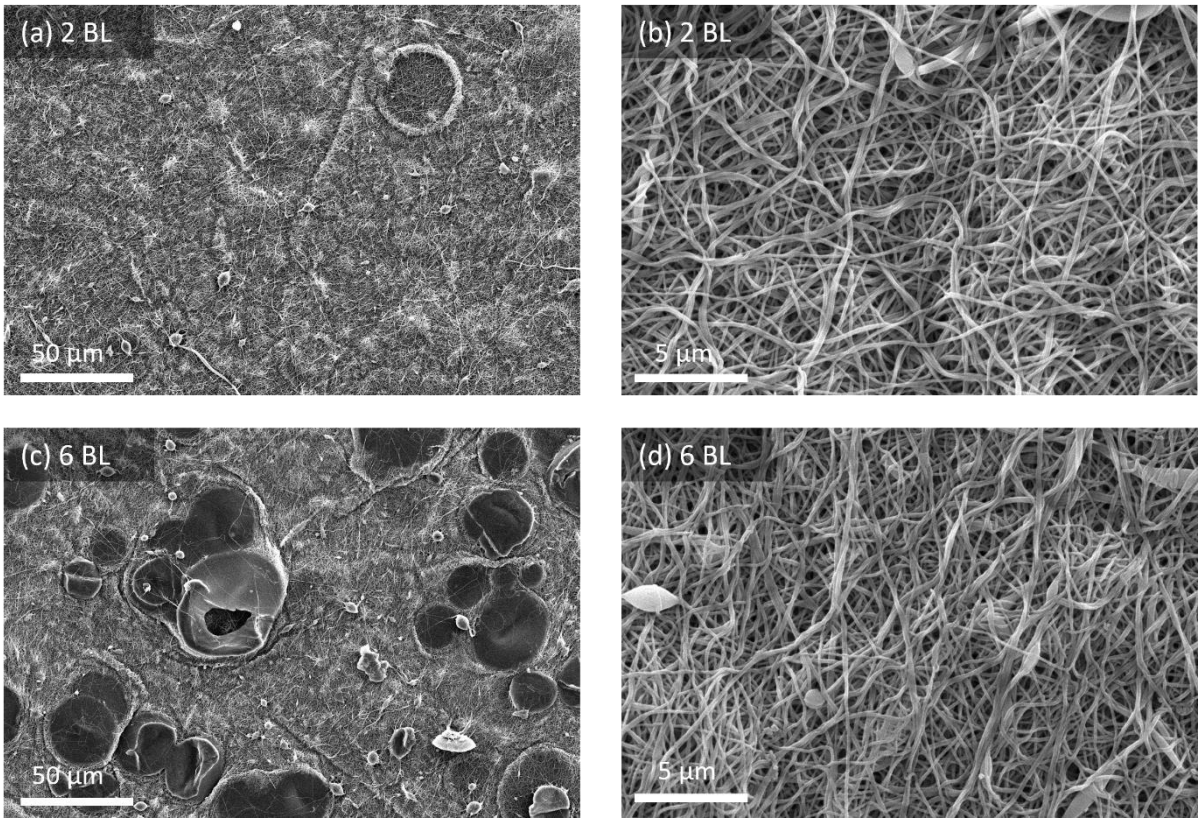

Figure 4.5 Scanning electron micrographs of layer-by-layer coated SPEEK nanofiber mats with 0.01 wt% PEI and PAA in 50 mM NaCl solution at a pH of 6.5 for 2 bilayers (BL) (a: 500x; b: 5000x) and 6 BL (c: 500x; d:5000x).

Figure 4.5c shows the surface of the SPEEK fiber network after it has been coated with 6 bilayers of PEI and PAA. The structure of the fibers looks similar to that of the SPEEK mat coated with 2 bilayers, however, large droplets are observed. These images were taken from the side of the SPEEK mat that was directly in contact with the substrate during electrospinning. Directly on the substrate the solvent does not have enough time to evaporate and the fibers stay wet, resulting in the fusion of the polymer fibers into droplets that eventually solidify. The droplets do not seem to have been formed during the coating procedure, as these droplets are also seen in some other batches of pristine electrospun SPEEK mats. Figure 4.5d again shows how the fibers have swollen after coating with 6 bilayers. Swelling of the coated nanofibers will most likely not influence the performance of the BPM, as densification with hot pressing completely removes the fibrous structure.

4.2.3. BPM morphology

After electrospinning of SPEEK and FAA-3 and LbL coating of SPEEK, the nanofiber mats were assembled as was shown in Figure 3.3 in the experimental. The LbL modified SPEEK mat was sandwiched in between pristine SPEEK and FAA-3 mats and hot pressed at 150°C at 100 kN for 30 – 60 minutes. Figure 4.6a shows the assembled SPEEK and FAA-3 nanofiber mats on a Teflon sheet before going into the hot press. Figure 4.6b shows the densified BPM after 30 minutes of hot pressing at 100 kN and 150°C.

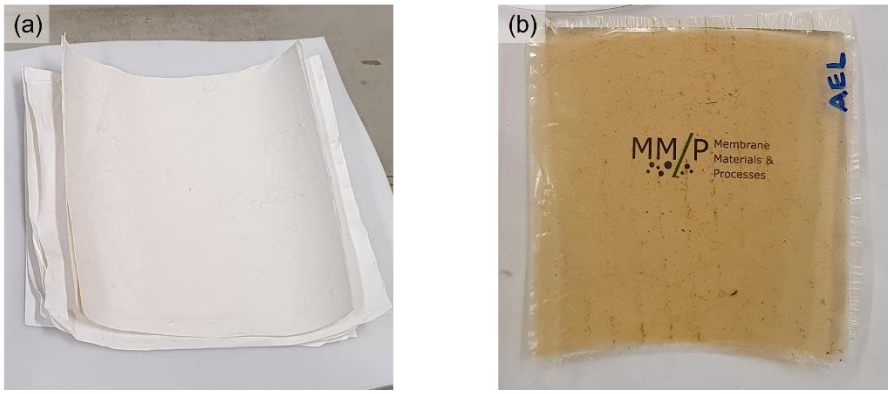

Figure 4.6 Pictures of (a) the assembled SPEEK and FAA-3 nanofiber mats with the FAA-3 mats on top and (b) the densified BPM after hot pressing at 100 kN at 150°C for 30 minutes.

The BPM has become completely transparent, indicating that after hot-pressing a dense structure is obtained. Some dark lines and speckles are visible across the membrane. These are either caused by dust particles that were settled on one of the nanofiber mats before hot pressing or they are artifacts from the spacer that was used to hold the membrane in place during the coating procedure.

Figure 4.7 shows SEM-EDX images of the cross-section of the hot pressed electrospun BPM. The SEM image of the cross-section shown in Figure 4.7a shows that the BPM is completely dense, as no pores or fibers are observed. It is clear from the image that the cross-section is composed of two phases with a sharp boundary. To determine which layer consists of which material, elemental mapping was performed with EDS. The elements that were mapped are sulfur and bromide. Sulfur was chosen because the element is unique to SPEEK, as it contains -SO_3H groups. Bromide is used as the counter-ion for the quaternary ammonium groups in FAA-3. In Figure 4.7b the EDS mapping of sulfur (yellow) is shown. Sulfur is only found in the top half of the BPM, indicating that the top polymer layer consists of SPEEK and is the CEL. In Figure 4.7c the elemental mapping of bromide (blue) is shown. Bromine is only found in the bottom half of the BPM, indicating that this part consists of FAA-3 and is the AEL. Unfortunately, it was not possible to visualize the presence of the LbL coated PEI and PAA layers. PEI and PAA contain similar elements as SPEEK and FAA-3 and the amount of adsorbed PE was too little compared to the bulk to give a significant signal.

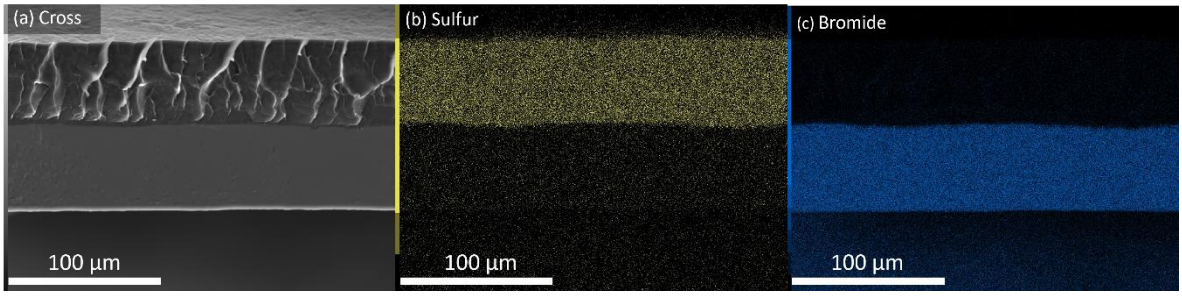

Figure 4.7 SEM-EDS images of the BPM after hot pressing: (a) SEM image of the cross-section of the hot pressed electrospun BPM; (b) elemental mapping for sulfur; (c) elemental mapping for bromide.

The benefit of using electrospinning for BPM fabrication is that it yields a heterogeneous IL with an entangled network of polymer nanofibers. In literature, dual fiber electrospinning was used to obtain a 3D junction, where the cation and anion exchange polymer were spun simultaneously.[35,36,39] The wire-electrospinner used in this work was, unfortunately, incapable of spinning two different polymers at the same time. This limits the thickness of the 3D junction that could be obtained. However, since the nanofiber mats are highly porous, hot pressing near the T_g of SPEEK and FAA-3

leads to fusion of the nanofibers in the IL and still results in an entangled network. The thickness of the 3D junction was estimated by extracting the elemental profiles from the SEM-EDS images in Figure 4.7 using ImageJ and the result is shown in Figure 4.8.

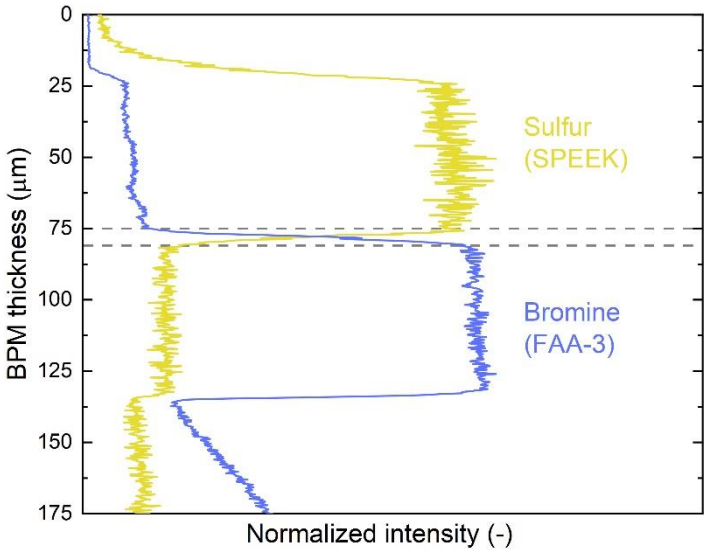

Figure 4.8 Elemental mapping profiles of sulfur (SPEEK) and bromide (FAA-3) obtained from EDS images of the cross section of a hot pressed electrospun BPM. The dashed lines indicate the overlap of SPEEK and FAA-3 and estimate the thickness of the 3D junction.

The elemental profiles show that the densified BPM is roughly 125 µm thick. The CEL (SPEEK) and AEL (FAA-3) have about the same thickness. The thickness of the 3D junction is determined from the amount of overlap between the SPEEK and FAA-3 profiles and is estimated to be approximately 6 µm. As the thickness of the 3D junction gets larger, the entanglements between the CEL and AEL increases, resulting in a higher interfacial area. The larger interfacial surface area promotes adhesion and enhances WD by providing multiple pathways for the WD products to leave the junction towards their respective IELs.[35,39,40] However, increasing the 3D junction thickness decreases the electric field strength established between the AEL and CEL, which in turn decreases the WD rate enhancement according to the second Wien effect (SWE).[68] Incorporation of a catalyst layer in the bipolar junction is also shown to decrease the electric field strength as the amount of catalyst increases.[40,52,102] The thickness of the 3D junction and the amount of catalyst that is added to the junction should therefore be carefully tuned in order to maximize the advantages both provide.

4.3. Membrane performance

The effect of the LbL modification of the interface layer (IL) of electrospun BPMs on the BPM performance was assessed by systematically varying the coating conditions used for the buildup of PEI and PAA multilayers. In total, 13 BPMs were prepared with different number of bilayers, different PE concentrations and using different ionic strength and pH values of the coating solutions. The water dissociation (WD) performance of these BPMs was evaluated by the recording of polarization curves and by measuring the permselectivity.

4.3.1. Polarization behavior

All polarization were recorded by applying current densities from 0 – 10 mA cm^{-2} and measuring the transmembrane potential drop in 0.5 M NaCl solution. Several interesting properties of the BPM can be extracted from the polarization curves, such as the area specific resistance (ASR), the WD onset potential (U_{WD}) and the limiting current density (i_{lim}). Figure A-4 shows how these properties are obtained from the polarization curves.

4.3.1.1. Effect of the number of bilayers and the PE concentration

The effect of the number of bilayers and the PE concentration was evaluated by preparing six BPMs at PE concentrations of 0.01 and 0.1 wt% in 50 mM NaCl solution at a pH of 6.5 and by varying the number of bilayers between two and six. The LbL modified BPMs were compared to a unmodified electrospun BPM (0 BL). The resulting polarization curves are shown in Figure 4.9. ASR and U_{WD} of the BPMs are shown in Table 4.2, together with the total adsorbed amount of PE, as determined by optical reflectometry on a silicon wafer.

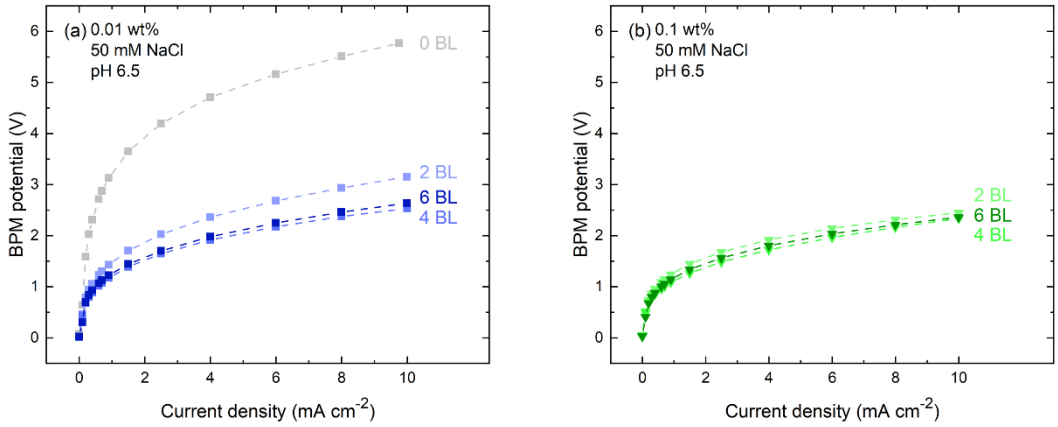

Figure 4.9 Polarization curves of prepared BPMs, modified by LbL application of two, four and six bilayers (BL) of PEI and PAA at PE concentrations of (a) 0.01 wt% and (b) 0.1 wt% in 50 mM NaCl solutions at a pH of 6.5. Current densities were applied between 0 – 10 mA cm^{-2} in 0.5 M NaCl solution.

Figure 4.9a shows the polarization curves measured for the BPMs that were modified with two, four and six bilayers (2 BL, 4 BL and 6 BL, respectively) of 0.01 wt% PEI and PAA in 50 mM NaCl and at a pH of 6.5. The performance of the LbL modified BPMs is compared to a reference BPM without any PE in the IL (0 BL). The reference BPM shows a significantly higher transmembrane potential than the modified membranes and therefore has the worst performance. At 0 BL, no catalytically active functional groups are present in the IL and the WD reaction is only accelerated by the SWE. The addition of only two bilayers of PEI and PAA under these conditions already decreases U_{WD} by 2.23 V and the ASR by 43.45 Ω cm^2, as can be seen in Table 4.2. That indicates the that introduction of PEI and PAA multilayers to the IL effectively promotes water dissociation. When increasing the number of

bilayers from two to four, a further increase of the WD performance is observed. The reflectometry data showed that increasing the number of bilayers also increases the total adsorbed amount of PE. With an increased amount of PE present in the IL, the number of weakly acidic and basic functional groups also increases. thus catalytically active sites also increases. The total adsorbed amount of PE showed linear growth as a function of the number of bilayers at 0.01 wt%, 50 mM NaCl and a pH of 6.5 (Figure 4.2). Therefore, a linear increase in WD performance was expected. However, when the number of bilayers was increased from four to six, the obtained polarization curve of 6 BL barely differs from the polarization curve of 4 BL. The performance even slightly decreases, as can be seen from the increasing ASR and U_{WD} in Table 4.2. This is an unexpected result, because the BPM performance did increase when the number of bilayers was increased from two to four and the reflectometry data showed that adding more bilayers increases the total adsorbed mass. A preliminary explanation was that the initial coating procedure was faulted.

Table 4.2 Variation of the total PE adsorption, as determined by optical reflectometry on a silicon wafer, the water dissociation onset potential (U_{WD}) and the area specific resistance (ASR) of BPMs with 0 – 6 BL of PEI and PAA, prepared at PE concentrations of 0.01 wt% and 0.1 wt% in 50 mM NaCl at a pH of 6.5.

Bilayers (#)	Tot. ads. (mg m^{-2})		U_{WD} (V)		ASR (Ω cm^2)	
	0.01 wt%	0.1 wt%	0.01 wt%	0.1 wt%	0.01 wt%	0.1 wt%
0 BL	0.00		4.28		161.57	
2 BL	1.85	1.54	2.05	1.73	118.12	76.67
4 BL	4.40	3.93	1.69	1.47	90.2	92.89
6 BL	6.38	5.72	1.72	1.59	97.14	81.78

During the preparation of the first set of LbL BPMs the same coating solution was used for each coating step. The coating baths contain a finite amount of PE, which obviously reduces after each coating step. Since there is a maximum in the performance at four bilayers, these results suggest that the coating solutions were depleted of PE and no more adsorption took place somewhere between two and six bilayers. To find out whether this was indeed the case, new coating solutions were prepared. The ionic strength and pH remained at 50 mM NaCl and 6.5, but the PE concentration was increased to 0.1 wt%. Also, the solutions were refreshed after each adsorption step to ensure a sufficient amount of PE was available for adsorption. New BPMs with two, four and six bilayers were prepared with the updated coating procedure and their electrochemical performance was assessed.

The polarization curves of the BPMs prepared in 0.1 wt% PE solutions are shown in Figure 4.9b. The LbL modified BPMs again outperform the reference BPM significantly, with a decrease in U_{WD} of more than 2.5 V compared to the 0 BL. The BPMs prepared at 0.1 wt% with the new procedure do seem to perform slightly better than the BPMs prepared at 0.01 wt%, indicating that the updated coating procedure improves the PEM formation and thus the BPM performance. However, the linear performance increase that was expected with the deposition of more bilayers was not observed. It seems that the extra PE that is present when more bilayers are added under these conditions is not enough to induce a significant performance increase. This explanation becomes more plausible when the effect of ionic strength is investigated.

4.3.1.2. Effect of ionic strength of the coating solutions

To analyze the effect the ionic strength of the coating solutions has on the performance of the LbL modified BPMs, BPMs were prepared using coating solution with ionic strengths of 5, 50 and 500 mM NaCl. The results of the previous section showed that increasing the PE concentration from 0.01 wt% to 0.1 wt% did not significantly improve the BPM performance. Therefore, six bilayers were deposited

at a PE concentration of 0.01 wt% while refreshing the coating solutions in each step. The pH of the coating solutions was adjusted to 6.5, PEI and PAA both have a high ionization degree at this pH. This ensured that the BPM performance was exclusively determined by the effect that the ionic strength has on the PEM growth. Polarization curves were recorded in 0.5 M NaCl solution and are shown in Figure 4.10. The total adsorbed amount of PE, U_{WD} and ASR are shown in Table 4.3.

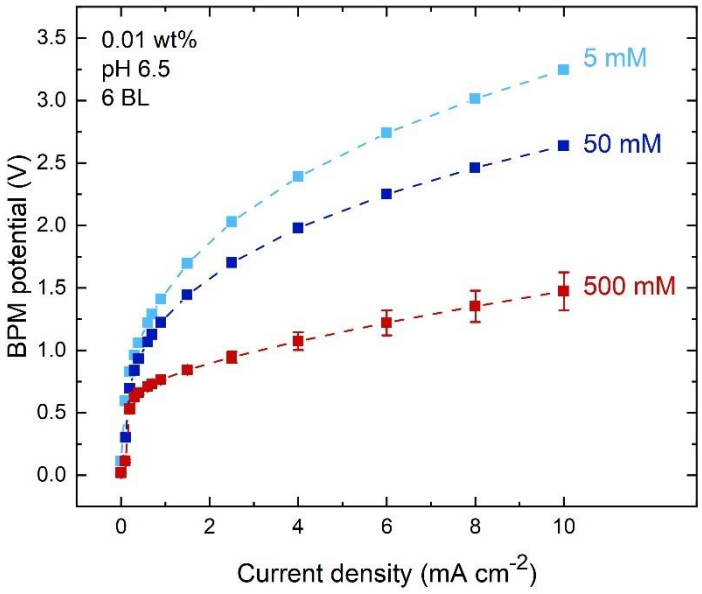

Figure 4.10 Polarization curves of prepared BPMs, modified by LbL application of six bilayers of PEI and PAA at a PE concentration of 0.01 wt% in 5, 50 and 500 mM NaCl solutions at a pH of 6.5. Current densities were applied between 0 – 10 mA cm^{-2} in 0.5 M NaCl solution.

Figure 4.10 shows the transmembrane potential drop significantly for the LbL BPMs prepared with six bilayers of PEI and PAA with increasing ionic strength. The 5 mM BPM shows the worst performance, with a U_{WD} of 2.08 V and an ASR of 126.43 Ω cm^2. Upon increasing the ionic strength to 50 mM, the U_{WD} decreases to 1.72 V and the ASR decreases to 97.14 Ω cm^2. Then when the ionic strength is increased to 500 mM NaCl, the WD performance increases drastically. The U_{WD} decreases down to 0.86 V, which is very close to the theoretical U_{WD} and ASR reduces by almost 50% to 63.5 ± 12.46 Ω cm^2.

Table 4.3 Variation of the total PE adsorption, as determined by optical reflectometry on a silicon wafer, the water dissociation onset potential (U_{WD}) and the areaspecific resistance (ASR) of BPMs with 6 BL of PEI and PAA, prepared at a PE concentration of 0.01 wt% in 5, 50 and 500 mM NaCl at a pH of 6.5.

[NaCl] (mM)	Tot. ads. (mg m^{-2})	U_{WD} (V)	ASR (Ω cm^2)
5	1.86	2.08	126.43
50	6.38	1.72	97.14
500	28.5	0.86 ± 0.02	63.5 ± 12.46

Making the LbL modified BPMs was a very time consuming process. Because the BPM prepared at 500 mM NaCl showed such enhanced WD performance, this BPM was prepared in duplicate. Therefore, it is the only polarization curve that shows error bars. The polarization curves of all BPMs were recorded in triplicate and the values shown are the average potentials of the last two measurements, which

were all within a 5% error margin. Figure 4.10 and Table 4.3 show a clear correlation between the ionic strength of the coating solutions, the total adsorbed amount of PE and the WD performance. All BPMs are coated with six bilayers of PEI and PAA. However, the total adsorbed amount of PEI and PAA increases with increasing ionic strength. This is a result of the different types of charge compensation that occur during PEM growth. PEI and PAA chains adopt linear conformations at low ionic strengths (5 and 50 mM NaCl), leading to the charges primarily being intrinsically compensated. This results in the deposition of thin layers and thus lower total adsorption. At higher ionic strengths (500 mM NaCl), the charges are extrinsically compensated. This results in exponential PEM growth and therefore a higher catalyst loading. With more PE present, more weakly basic and acidic functional groups are present in the IL to catalyze the WD reaction.

Since the BPM with 6 BL at 500 mM NaCl showed such improved WD performance, an attempt was made to increase the WD performance even more by doubling the number of bilayers. Before the BPM was prepared, the PEM growth was studied up to 12 bilayers (12 BL) with optical reflectometry. The resulting adsorption curve is plotted next to the original adsorption curve of up to six bilayers in Figure 4.11a. Since the same conditions were used for both measurements, it was expected that the adsorption curve would follow the same trend up to six bilayers. However, this is not the case. The adsorption curve of 12 BL follows that of 6 BL for the first two bilayers, but then it starts to deviate. Whereas the PEM of 6BL showed exponential growth for all bilayers, the PEM of 12 BL grows linearly between 3 and 7 bilayers and only then starts growing exponentially. As Figure 4.11a shows, 10 bilayers are needed to reach a total adsorption equal to that of the 6 BL after six bilayers. The exact reason for the big difference in adsorption is still unclear. The measurement was performed twice with the same solutions, but again there were large deviations in adsorption, as shown by the large error bars. The only parameter that was changed in the measurement was the silicon wafer that was used for the adsorption of the multilayers. The thickness of the SiO_2 layer significantly influences the output signal of the reflectometer. It was later found that there were large deviations in the thicknesses of the SiO_2 top layers between strips of the same wafer. The calculations, however, were performed with the average top layer thickness. That might explain the big difference in the adsorption curves. Nevertheless, the total adsorption after 12 bilayers increased by more than 60% compared to the 6 BL.

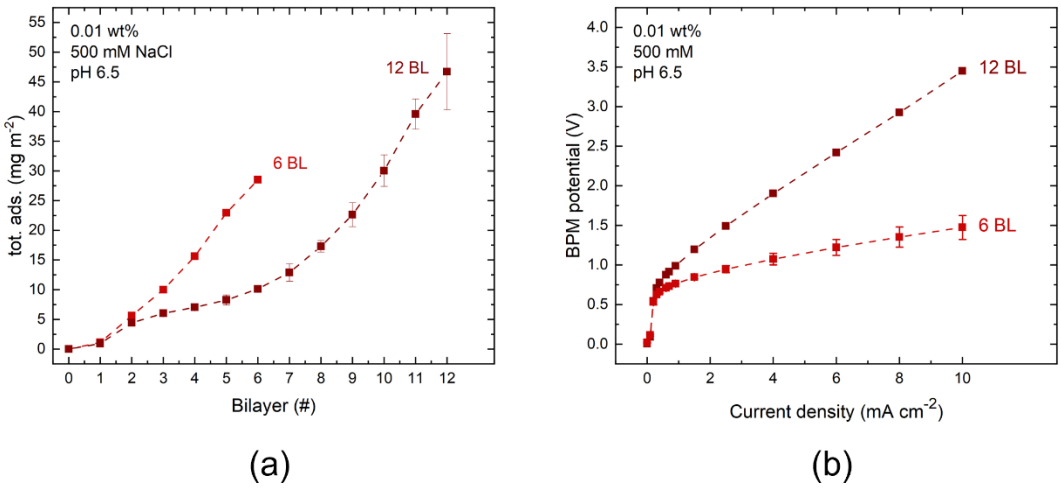

Figure 4.11 (a) Adsorption curve of PEI and PAA at concentrations of 0.01 wt% in 500 mM NaCl at a pH of 6.5 determined with optical reflectometry and (b) polarization curves recorded in 0.5 M NaCl of LbL BPMs prepared with six and 12 BL of PEI and PAA at concentrations of 0.01 wt% in 500 mM NaCl at a pH of 6.5.

With a total PE adsorption of 46.7 mg m^{-2} it was expected that the 12 BL BPM would perform better than the 6 BL BPM. However, Figure 4.11b shows that the increased number of bilayers has had a negative impact on the WD performance. At 0.94 V, the U_{WD} of the 12 BL BPM is relatively low and approaches that of the 6 BL at 0.86 V. However, the ASR (257.93 Ω cm^2) has increased drastically compared to the 6 BL (63.5 $\pm$ 12.46). The relatively low U_{WD} can be attributed to the high PEI and PAA loading at 46.7 mg m^{-2}. The high amount of catalytic sites lowers the activation energy for WD and thus the onset potential. As the WD reaction takes place at these catalytic sites, it was assumed that the increased loading would increase the amount of charge carriers and thus lower the ohmic resistance. The high ASR can possibly be explained by comparing the SEM images taken from the LbL SPEEK nanofiber mat coated with 6 bilayers and 12 bilayers, shown in Figure A-5. While the fiber network in Figure A-5a has stayed intact, indicating that each fiber has been coated individually, Figure A-5b shows that the PEM seems to be deposited on top of the fiber network as a thick film. The bulk of a PEM consists of a neutral region where the charges on the PEs are stoichiometrically compensated and is therefore assumed to be charge neutral.[94] Introducing a neutral region to the interface layer (IL) increases the width of the space charge region (SCR), which in turn lowers the electric field strength in the IL. This decreases the water splitting rate according to the second Wien effect (SWE) and leads to a higher resistance.[52] The thick, neutral region in the IL also provides a longer pathway for the WD products to reach the IELs.[65] Together with the reduced electric field strength, this might increase the occurrence of water recombination in the IL, also adding to the increased ASR. From these results it becomes evident that adding more catalyst to the IL by simply adding more bilayers does not necessarily increase the WD performance. There seems to be a tradeoff between the amount of catalytic sites and the thickness of the PEM, as it has been shown that too high catalyst loadings can negatively impact the WD performance.[44,65]

Table 4.4 Variation of the total PE adsorption, as determined by optical reflectometry on a silicon wafer, the water dissociation onset potential (U_{WD}) and the area specific resistance (ASR) of BPMs with 6 and 12 BL of PEI and PAA, prepared at a PE concentration of 0.01 wt% in 500 mM NaCl at a pH of 6.5.

Bilayers (#)	Tot. ads. (mg m^{-2})	U_{WD} (V)	ASR (Ω cm^2)
6	28.5	0.86 $\pm$ 0.02	63.5 $\pm$ 12.46
12	46.7	0.94	257.93

4.3.1.3. Effect of pH of the coating solutions

Besides the effect of the ionic strength, the effect of the coating solution pH on the BPM performance was assessed. The PEI and PAA multilayer growth can be controlled by varying the pH of the coating solutions, as was shown in section 4.1.2. Since the reflectometry results of pH 4/4 and 10/3.7 showed the highest total PEI and PAA adsorption, LbL BPMs were prepared at 0.01 wt% PEI and PAA and 50 mM NaCl. Polarization curves were recorded by applying current densities between 0 – 10 mA cm^{-2} and measuring the potential drop across the BPM. The resulting curves are shown in Figure 4.12.

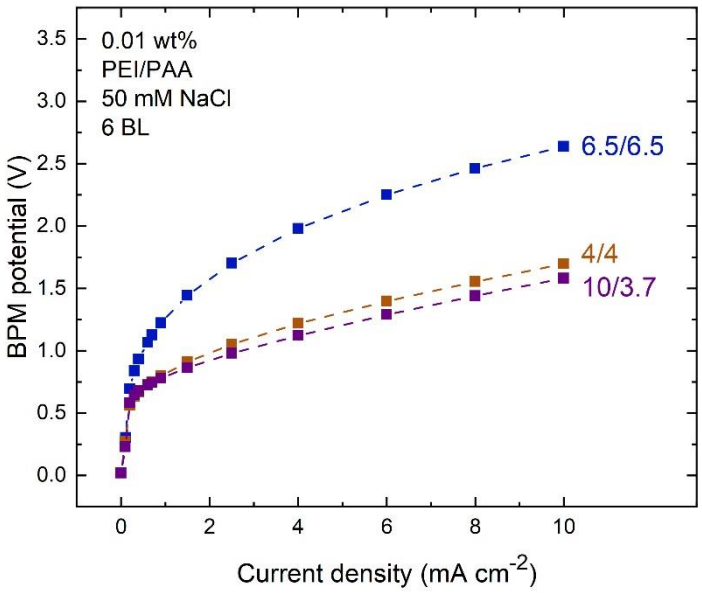

Figure 4.12 Polarization curves of prepared BPMs, modified by LbL application of six bilayers of PEI and PAA at a PE concentration of 0.01 wt% in 50 mM NaCl solutions at a pH (PEI/PAA) of 6.5/6.5, pH 4/4 and pH 10/3.7. Current densities were applied between 0 – 10 mA cm^{-2} in 0.5 M NaCl solution.

Figure 4.12 shows the potential drop over the BPM as a function of current density. The pH values of, respectively, the PEI and PAA coating solutions used for the preparation of the BPMs are depicted at the end of each polarization curve. The pH, total PE adsorption after six bilayers, U_{WD} and ASR are summarized in Table 4.5. Similar to the BPMs prepared at varied ionic strengths, the WD performance increases as the total adsorbed amount of PEI and PAA increases. At pH 6.5/6.5 the PEI and PAA multilayer grows linearly, hence the relatively low total adsorption of 6.38 mg m^{-2}. At pH 4/4 exponential growth of the PEM occurs and the total adsorption is significantly higher after six bilayers compared to pH 6.5/6.5. As the adsorption increases from 6.38 mg m^{-2} to 24.99 mg m^{-2}, the U_{WD} decreases from 1.72 V to 0.98 V and ASR decreases from 97.14 Ω cm^2 to 74.85 Ω cm^2. The performance increase can be attributed to the increased amount of weakly basic and acidic functional groups present in the IL, which catalyze the WD reaction.[62] As the pH changes from 4/4 to 10/3.7, the total PE adsorption increases from 24.99 mg m^{-2} to 30.02 mg m^{-2}. This results in a decrease of U_{WD} from 0.98 V to 0.87 V and ASR decreases only slightly from 74.85 Ω cm^2 to 73.11 Ω cm^2. The decrease of U_{WD} can again be attributed to the increased amount of catalytically active functional groups on PEI and PAA. The only slight improvement of the ASR could arguably be explained by the increased thickness of the PEM. As the catalyst layer in the bipolar junction gets thicker, the electric field strength decreases.[52] The WD rate decreases as a result, offsetting some of the benefits gained from the increased PE content.

Table 4.5 Variation of the total PE adsorption, as determined by optical reflectometry on a silicon wafer, the water dissociation onset potential (U_{WD}) and the area specific resistance (ASR) of BPMs with 6 BL of PEI and PAA, prepared at a PE concentration of 0.01 wt% in 50 mM NaCl at different pH.

pH (PEI/PAA)	Tot. ads. (mg m^{-2})	U_{WD} (V)	ASR (Ω cm^2)
6.5/6.5	6.38	1.72	97.14
4/4	24.99	0.98	74.85
10/3.7	30.02	0.87	73.11

It is a noteworthy result that the total adsorption and PEM growth of the BPMs with six bilayers prepared at 50 mM NaCL at pH 4/4 and 10/3.7 is very similar to that of the BPM with six bilayers prepared at 500 mM NaCl at pH 6.5 and that these three BPMs show very similar performance. This suggests that there is a correlation between the PE adsorption and BPM performance. This correlation will be further explored in the following section.

4.3.1.4. Effect of total PE adsorption

In order to find a correlation between the PE adsorption and the WD performance, the U_{WD} and ASR of the LbL modified BPMs are plotted as a function of the total adsorbed amount of PEI and PAA. These results are shown in Figure 4.13a and Figure 4.13b, respectively. In Figure 4.13a, a clear downward trend in U_{WD} is visible with increasing total adsorption. With only small amounts of PE adsorption, the U_{WD} decreases drastically. Then, when the total adsorption increases from around 5 mg m^{-2} towards 25 – 30 mg m^{-2}, the U_{WD} values decrease slightly further until they seem to reach a plateau. That suggests that simply adding more PE to the IL does not necessarily increase the WD performance. The polarization curves in Figure 4.9 already demonstrated that adding more bilayers did not improve the WD performance, even though the total adsorption increased. Something similar happens in the high adsorption range, where the total adsorption increases from 25 – 30 mg m^{-2}, but the differences in U_{WD} are negligible. In the lower adsorption range the PEI and PAA multilayer grows linearly, leading to dense, but smooth multilayers. In the high adsorption range, exponential PEM growth occurs, leading to more open multilayers with a rough surface. This was demonstrated by Yuan et al.[97], where atomic force microscopy and field emission SEM images were taken from PEI and PAA multilayers grown under very similar circumstances. This leads to the hypothesis that it is not the entire PEM that contributes to the acceleration of the WD reaction, but only the outer surface of the multilayer. According to the "three zone model" proposed by Ladam et al.[94], a PEM can be divided into three zones. The first zone consists of the layers that are deposited directly onto the substrate. These layers have different properties than those in zone two and three. Zone two is called the "bulk" zone, where the charges on the PEs are stoichiometrically compensated. Zone three is the layer that is closest to the outer surface of the multilayer. The functional groups of the layers in zone three are not compensated and therefore still charged. The charged functional groups are the groups that are hypothesized to be catalytically active and contribute to the acceleration of the WD reaction.[33,61] Exponential PEM growth therefore not only increases the total PE adsorption, but it also increases the roughness of the PEM surface, which in turn contributes to the acceleration of the WD reaction.

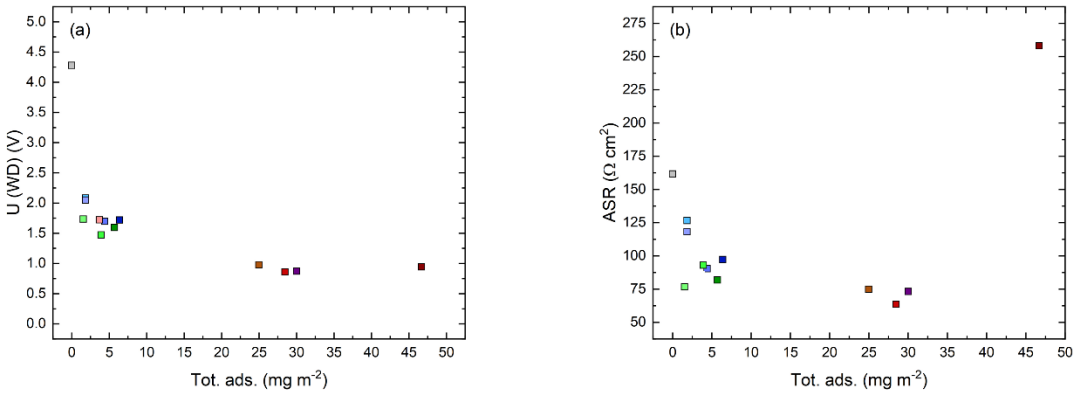

Figure 4.13 Correlation between the total adsorbed amount of PEI and PAA and (a) the water dissociation onset potential (U_{WD}) and (b) the area specific resistance (ASR) of all prepared and tested LbL modified BPMs.

A similar trend as for the U_{WD} is observed for the ASR in Figure 4.13b. As the total adsorbed amount of PEI and PAA increases to 30 mg m^{-2}, the ASR decreases. Again, a sharp decrease is seen in the smaller range from 0 to around 5 mg m^{-2}. The WD reaction is catalyzed already at low PEI and PAA loadings, as evidenced by the U_{WD} decrease found in Figure 4.13a. The resulting increased flux of H^+ and OH^- ions drastically increases the amount of charge carriers in the IL, which in turn reduces the ASR. As the total adsorption increases further, the ASR decreases only slightly. Then, around a total adsorption of 45 mg m^{-2}, the ASR increases drastically. This "U-shaped" dependence of the resistance on the catalyst loading was also found by Chen et al[65], where they reasoned that thicker catalyst layers would increase the ionic resistance. The PEM with a total adsorption of around 45 mg m^{-2} consisted of 12 bilayers and was formed in 500 mM NaCl solution at a pH of 6.5. It was shown in Figure A-5 that, in this case, the PEM was partly formed as a film on top of the SPEEK nanofibers, instead as a coating around the fibers. It could be reasoned that this increases the thickness of the layer and thus drastically increases the ionic resistance.

Based on these data, the best WD performance was achieved for the BPMs with a PE loading of around 30 mg m^{-2}. These were the BPMs with 6 BL that were prepared at 500 mM NaCl solution at a pH of 6.5, and in 50 mM NaCl solutions at pH values of 4/4 and 10/3.7. Even though they were prepared under different conditions, the reflectometry data showed very similar growth of the PEI and PAA multilayer. This suggests that the performance of the LbL modified BPMs really depends on the type of PEM growth and the final structure of the PEM, independent of the conditions used to grow the multilayer. This also means that both the ionic strength and pH of the coating solutions can be used to tweak the performance of electrospun BPMs.

4.3.2. Apparent permselectivity

The apparent permselectivity describes the ability of an IEM to discriminate between ions of opposite charge and is a measure of the amount of unwanted co-ion crossover.[103] The permselectivity for monopolar IEMs is usually determined by measuring the OCV across an IEM placed in between 0.1 and 0.5 M KCl solutions.[104] The permselectivity then describes the magnitude of crossover of K^+ ions, in the case of an AEM, from the high concentration compartment to the low concentration compartment. In the case of a CEM the magnitude of the crossover of Cl^- ions is determined. SPEEK and FAA-3 are known to have excellent permselectivities towards CL^- and Na^+, respectively.[30,39] This is reflected in the apparent absence of an Ohmic region in the polarization curves at low current densities and low limiting current densities. In BPMs however, ion leakage is more likely to occur for the more mobile OH^- and specifically H^+ ions. [30,39] The permselectivity of BPMs is therefore determined by measuring the OCV across a BPM separating a 0.5 M HCl and 0.5 M NaOH solution. In this case, the permselectivity is a measure of the amount of crossover of H^+ and OH^- ions that occurs through the AEL and CEL, respectively. The permselectivity is then determined as the ratio between the measured OCV and the theoretical OCV calculated with the Nernst equation (Eq. 3.3), which is 0.775 V. The results of these measurements are plotted in Figure 4.14. The measured OCV and the permselectivity calculated from this value are plotted on the left and right axis, respectively.

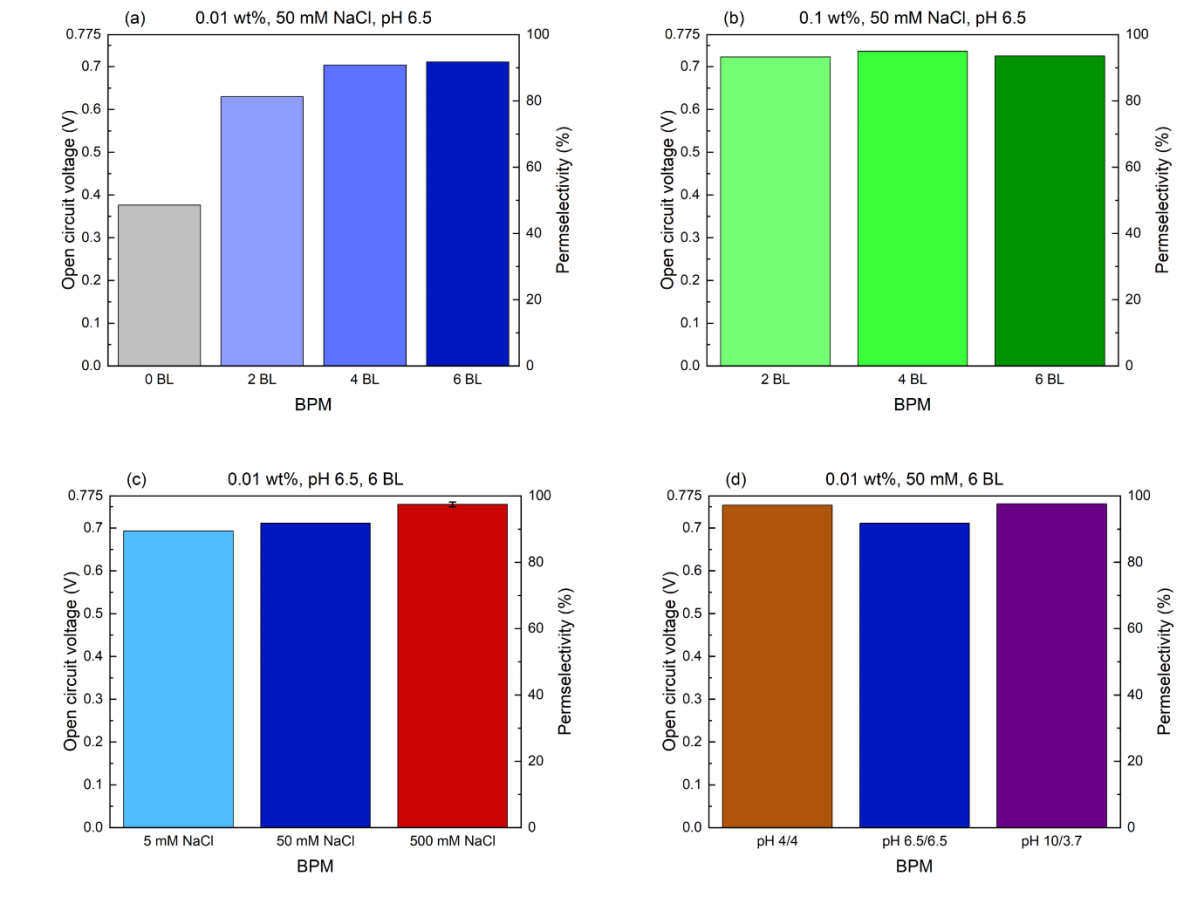

Figure 4.14 Measured open circuit voltage (OCV) and corresponding permselectivity of the electrospun LbL modified BPMs in 0.5 M HCl and NaOH solutions. The BPMs were prepared in the following conditions: (a) 0.01 wt% PEI and PAA, 50 mM NaCl, pH 6.5, 2 – 6 bilayers (BL); (b) 0.1 wt% PEI and PAA, 50 mM NaCl, pH 6.5, 2 – 6 BL; (c) 0.01 wt% PEI and PAA, 5 – 500 mM NaCl, pH 6.5, 6 BL; (d) 0.01 wt% PEI and PAA, 50 mM NaCl, pH 4/4, 6.5/6.5 and 10/3.7.

SPEEK and FAA-3 are known to have good permselectivity for Na^+ and Cl^-.[30,39] The OCV in BPMs, however, is a measure of the selectivity of the IELs towards H^+ and OH^- ions. BPMs should have high permselectivity towards protons and hydroxyl ions in order to maintain a stable pH gradient across the BPM for when it is used in energy applications, such as acid-base flow batteries[37] or water electrolysis.[105] Figure 4.14a, shows the OCV values and corresponding permselectivities for BPMs with 0 – 6 BL prepared in 50 mM NaCl at a pH of 6.5. At 0 BL, the permselectivity is only determined by the permselectivities of the respective IELs, since there is no catalyst present in the IL. As a result, a low permselectivity of about 50% is observed for the 0 BL BPM. This low value can possibly be explained by H^+ leakage through the AEL, since FAA-3 is known to swell significantly in water.[106] The permselectivity is dependent on the charge density of the IEL.[103] As FAA-3 swells, the charge density effectively decreases and results in a lower permselectivity. The permselectivity increases significantly after addition of the first two bilayers of PEI and PAA. As the number of bilayers increases, the permselectivity is also observed to increase. Each added bilayer increases the charge density in the IL, as PEI and PAA contain charged functional groups. As a result, the permselectivity increases, until the highest value of 92% is achieved for the 6 BL. The effect of the increasing number of bilayers is less pronounced when looking at the permselectivity of the BPMs prepared at 0.1 wt% PEI and PAA in Figure 4.14b. Here the permselectivity does increase from 2 to 4 BL, but then from 4 to 6 BL the permselectivity decreases slightly. However, a general increasing trend is observed between the number of bilayers and the permselectivity.

Then, in Figure 4.14c, the OCV values and apparent permselectivities of the BPMs prepared with 6 BL of 0.01 wt% PEI and PAA in 5, 50 and 500 mM NaCl at a pH of 6.5 are shown. The permselectivity is observed to increase with increasing ionic strength of the coating solutions. Since all three BPMs have six bilayers of PEI and PAA, the permselectivity is purely determined by the type and amount of adsorption that has occurred. The reflectometry data (Figure 4.2a) showed that the total adsorption increased as the ionic strength of the coating solutions increased. As the ionic strength increased, the charge compensation shifts from intrinsic to extrinsic, resulting in a transition from linear to exponential PEM growth. As a consequence, the deposited bilayers become thicker and more PE adsorbs per bilayer and the charge density in the IL therefore increases drastically. This explains the high permselectivity observed in the 500 mM BPM (97%), which is on par with the permselectivity of the commercially available Fumatech® FBM (98%). A similar explanation can be given for the high permselectivities observed in Figure 4.14d. Here the OCV values and permselectivities are plotted of the BPMs prepared with 6 BL of 0.01 wt% PEI and PAA in 50 mM NaCl at pH 4/4, 6.5/6.5 and 10/3.7. The reflectometry data showed exponential growth and a high total PE adsorption for both pH 4/4 and 10/3.7 (Figure 4.3). The observed apparent permselectivities are substantially higher (97% and 98%, respectively) than that of pH 6.5/6.5 (92%). Hence, these results suggest that both increasing the number of bilayers as well as increasing the thickness of each layer, which can be achieved by increasing the ionic strength or varying the pH of the coating solutions, increases the apparent permselectivity of LbL modified BPMs.

Chapter 5. Conclusion

This work aimed to accelerate the WD reaction in electrospun BPMs by incorporating PE catalysts into the IL via the LbL technique. The used PEs were PEI and PAA, as they contain catalytically active functional groups. The growth behavior of PEI and PAA multilayers was evaluated by optical fixed angle reflectometry. The results showed that the PEM growth could be controlled by varying the ionic strength and the pH of the coating solutions. The ionic strength of the coating solutions determines the type of charge compensation that occurs between the PEs. As PE charges are intrinsically compensated at low salt concentrations (5 and 50 mM NaCl), the PE chains are long and elongated, resulting linear PEM growth. At high salt concentrations (500 mM NaCl), PE charges are extrinsically compensated and the chains adopt coiled conformations due to screening of the charges. This drastically increases the adsorbed amount of PE per layer and increases the interdiffusion of PE into the PEM, resulting in exponential growth. The PEM growth is controlled in a similar manner via the pH of the coating solutions. Since PEI and PAA are weak PEs, their effective charge density can be controlled by varying their degree of ionization, which is dependent on the pH. It was shown that at pH values where the ionization degree was high, linear PEM growth was observed. As the ionization degree of especially PAA decreased, a shift occurred from linear to exponential growth, as the interdiffusion of PAA is higher at lower charge density. The highest total adsorption was found at pH values of PEI and PAA of 10 and 3.7, respectively. In this case, the ionization degree of both PEs was around 40%.

The PEI and PAA multilayers were incorporated into the BPMs by coating electrospun SPEEK nanofibers via the dip coating method. The LbL coated SPEEK mats were then sandwiched in between pristine electrospun SPEEK and FAA-3 mats, as the CEL and AEL, respectively. The stacks were densified via hot pressing, yielding BPMs with an entangles 3D junction of approximately 6 µm. The effect of the PEI and PAA multilayers on the WD performance was assessed by preparing BPMs with varying numbers of bilayers at different PE concentrations, ionic strength and pH of the coating solutions. The performance of the BPMs was assessed by recording polarization curves and measuring the permselectivity.

Interestingly, all LbL modified BPMs significantly outperformed the electrospun reference BPM, which contained no catalyst, showing the potential of PEI and PAA multilayers as a WD catalyst. A clear trend was observed between the WD performance and the total amount of adsorbed PEI and PAA, where only adding a small amount of PE already significantly improved performance. Optimum WD performance was found at a total adsorption around 30 mg m^{-2}. However, it is not necessarily the total amount of adsorbed PEI and PAA that determines the BPM performance, but also the structure and morphology of the PEM, since the functional groups on the outer layer of the PEM contribute to the catalysis of the WD reaction. These BPMs showed U_{WD} close to the thermodynamic limit (0.83V) and relatively low Ohmic resistances. These results were obtained from the BPMs prepared at 500 mM NaCl at a pH of 6.5 and for the BPMs prepared at 50 mM NaCl at pH values of 4/4 and 10/3.7. Even though the coatings were made under different conditions, the PEM growth behavior of these three BPMs was very similar, all showing exponential PEM growth. The permselectivities of these three BPMs were also significantly higher than the rest of the fabricated BPMs, being on par with commercial BPMs. The permselectivity was shown to increase when more bilayers were incorporated in the IL. In the BPMs with exponentially grown PEMs, however, the bilayers thicker than those in linearly grown PEMs. The BPM prepared with 12 BL in 500 mM NaCl at a pH of 6.5 demonstrated however that the amount of adsorbed PE could not increase the BPMs performance indefinitely.

Therefore, the number of bilayers, ionic strength and pH of the coating solutions should be tuned carefully in order to reach optimum WD performance.

Chapter 6. Outlook

Even though the LbL modified BPMs showed promising WD performance, there is still room for improvement. While the U_{WD} and permselectivity of the best performing BPMs were close to industry standard, the ASR values were high compared to the state-of-the-art.[40,41] In order to bring the ASR down, the IL should be further optimized. The best results were achieved by BPMs with exponentially grown PEMs up to six bilayers, but the performance decreased when the number of bilayers was doubled to 12 bilayers. It would be valuable to try and find the actual optimum performance by preparing BPMs with the complete range between 2 and 12 bilayers. Also, more reflectometry experiments should be performed to find the optimal combination of ionic strength and pH for maximal exponential PEM growth, since the functional groups on the outer surface of the PEM contribute to the catalysis of the WD reaction. All BPMs fabricated in this work were PAA terminated. PAA contains carboxylic acid groups, which were shown to be more catalytically active than the primary, secondary and tertiary ammonium groups on PEI. However, having a wide range of pK_a values available for WD should also lead to increased performance.[33] An interesting experiment would therefore be to prepare BPMs with PEI as the terminating layer.

Besides optimizing the coating conditions for PEI and PAA, the IL could be further optimized by tweaking the bipolar junction. In this work, BPMs were prepared by directly hot pressing the electrospun materials. Other researchers have shown, however, that DMF vapor treatment prior to hot pressing plasticizes the AEL and CEL and improves interfacial contact and reduces the energy barrier for WD. The 3D junction could also be further optimized by creating entangled network of SPEEK and FAA-3 fibers. In literature, this is accomplished by simultaneously spinning the cation and anion exchange material via dual fiber electrospinning.[35,39] Unfortunately, this was not possible with the wire-electrospinner used in this work. Something similar could be achieved, however, by spinning a thin layer of SPEEK on top of an existing FAA-3 nanofiber mat or vice versa. Something else that is worth it to explore is to use the AEL as a substrate to coat the PEM on, since it is known that WD primarily occurs in the AEL. In this work, this was not possible due to the excessive swelling of FAA-3 in water.

An important property of a BPM that was not discussed in this report is the current efficiency of the BPM. The current efficiency is defined as the fraction of the applied current that is actually used for the generation of protons and hydroxyl ions by the WD reaction. To gain more insight into the contributions of the WD reaction and the SWE to the resistance of the fabricated BPMs, electrochemical impedance spectroscopy could be applied, since the resistance extracted from the polarization curves could not discriminate between the two. Future work might also look at long term stability tests in both reverse and forward bias. Finally, it would be valuable to operate the BPMs at higher current densities. Due to limitations of the potentiostat, current densities above 10 mA cm^{-2} could not be achieved, while industrial current densities could go up to 1 A cm^{-2}. [33]

Bibliography

1 T. M. Letcher, Why do we have global warming?, *Managing Global Warming: An Interface of Technology and Human Issues*, 2018, 3–15.

2 T. M. L. Wigley, The pre-industrial carbon dioxide level, *Clim Change*, 1983, **5**, 315–320.

3 Daily CO2, https://www.co2.earth/daily-co2, (accessed 16 March 2023).

4 World of Change: Global Temperatures, https://earthobservatory.nasa.gov/world-of-change/global-temperatures, (accessed 16 March 2023).

5 IPCC, in *Global Warming of 1.5°C*, Cambridge University Press, 2022, pp. 1–24.

6 I. Energy Agency, Net Zero by 2050 - A Roadmap for the Global Energy Sector.

7 P. Sorknæs, R. M. Johannsen, A. D. Korberg, T. B. Nielsen, U. R. Petersen and B. V. Mathiesen, Electrification of the industrial sector in 100% renewable energy scenarios, *Energy*, , DOI:10.1016/J.ENERGY.2022.124339.

8 J. J. Anderson, D. C. Rode, H. Zhai and P. S. Fischbeck, Fossil-Fuel Options for Power Sector Net-Zero Emissions with Sequestration Tax Credits, *Cite This: Environ. Sci. Technol*, 2022, **2022**, 11162–11171.

9 P. D. Lund, J. Lindgren, J. Mikkola and J. Salpakari, Review of energy system flexibility measures to enable high levels of variable renewable electricity, *Renewable and Sustainable Energy Reviews*, 2015, **45**, 785–807.

10 M. H. Mostafa, S. H. E. Abdel Aleem, S. G. Ali, Z. M. Ali and A. Y. Abdelaziz, Techno-economic assessment of energy storage systems using annualized life cycle cost of storage (LCCOS) and levelized cost of energy (LCOE) metrics, *J Energy Storage*, , DOI:10.1016/J.EST.2020.101345.

11 R. Xia, S. Overa and F. Jiao, Emerging Electrochemical Processes to Decarbonize the Chemical Industry, *JACS Au*, 2022, **2**, 1054–1070.

12 H. Strathmann, Electrodialysis, a mature technology with a multitude of new applications, *Desalination*, 2010, **264**, 268–288.

13 K. Nagasubramanian, F. P. Chlanda and K. J. Liu, Use of bipolar membranes for generation of acid and base - an engineering and economic analysis, *J Memb Sci*, 1977, **2**, 109–124.

14 C. Fernandez-Gonzalez, A. Dominguez-Ramos, R. Ibañez and A. Irabien, Electrodialysis with Bipolar Membranes for Valorization of Brines, *Separation and Purification Reviews*, 2016, **45**, 275–287.

15 L. Monat, S. Chaudhury and O. Nir, Enhancing the Sustainability of Phosphogypsum Recycling by Integrating Electrodialysis with Bipolar Membranes, , DOI:10.1021/acssuschemeng.9b07038.

16 N. van Linden, G. L. Bandinu, D. A. Vermaas, H. Spanjers and J. B. van Lier, Bipolar membrane electrodialysis for energetically competitive ammonium removal and dissolved ammonia production, *J Clean Prod*, , DOI:10.1016/J.JCLEPRO.2020.120788.

17 X. Tongwen and Y. Weihua, Citric acid production by electrodialysis with bipolar membranes, *Chemical Engineering and Processing: Process Intensification*, 2002, **41**, 519–524.

18 X. Sun, H. Lu and J. Wang, Recovery of citric acid from fermented liquid by bipolar membrane electrodialysis, *J Clean Prod*, 2017, **143**, 250–256.

19 H. Ma, S. Yue, H. Li, Q. Wang and M. Tu, Recovery of lactic acid and other organic acids from food waste ethanol fermentation stillage: Feasibility and effects of substrates, *Sep Purif Technol*, 2019, **209**, 223–228.

20 X. Wang, Y. Wang, X. Zhang, H. Feng and T. Xu, In-situ combination of fermentation and electrodialysis with bipolar membranes for the production of lactic acid: Continuous operation, *Bioresour Technol*, 2013, **147**, 442–448.

21 X. Zhang, C. Li, Y. Wang, J. Luo and T. Xu, Recovery of acetic acid from simulated acetaldehyde wastewaters: Bipolar membrane electrodialysis processes and membrane selection, *J Memb Sci*, 2011, **379**, 184–190.

22 X. Vecino, M. Reig, O. Gibert, C. Valderrama and J. L. Cortina, Integration of Monopolar and Bipolar Electrodialysis Processes for Tartaric Acid Recovery from Residues of the Winery Industry, *ACS Sustain Chem Eng*, 2020, **8**, 13387–13399.

23 D. A. Vermaas and W. A. Smith, Synergistic Electrochemical CO2 Reduction and Water Oxidation with a Bipolar Membrane, *ACS Energy Lett*, 2016, **1**, 1143–1148.

24 Y. C. Li, D. Zhou, Z. Yan, R. H. Gonçalves, D. A. Salvatore, C. P. Berlinguette and T. E. Mallouk, Electrolysis of CO2 to Syngas in Bipolar Membrane-Based Electrochemical Cells, *ACS Energy Lett*, 2016, **1**, 1149–1153.

25 M. Ünlü, J. Zhou, P. A. Kohl, M. Ünlü, J. Zhou and P. A. Kohl, Hybrid Polymer Electrolyte Fuel Cells: Alkaline Electrodes with Proton Conducting Membrane, *Angewandte Chemie*, 2010, **122**, 1321–1323.

26 J. Xia, G. Eigenberger, H. Strathmann and U. Nieken, Flow battery based on reverse electrodialysis with bipolar membranes: Single cell experiments, *J Memb Sci*, 2018, **565**, 157–168.

27 J. H. Kim, J. H. Lee, S. Maurya, S. H. Shin, J. Y. Lee, I. S. Chang and S. H. Moon, Proof-of-concept experiments of an acid-base junction flow battery by reverse bipolar electrodialysis for an energy conversion system, *Electrochem commun*, 2016, **72**, 157–161.

28 A. Zaffora, A. Culcasi, L. Gurreri, A. Cosenza, A. Tamburini, M. Santamaria and G. Micale, Energy Harvesting by Waste Acid/Base Neutralization via Bipolar Membrane Reverse Electrodialysis, *Energies 2020, Vol. 13, Page 5510*, 2020, **13**, 5510.

29 S. Thiele, B. Mayerhöfer, D. McLaughlin, T. Böhm, M. Hegelheimer and D. Seeberger, Bipolar membrane electrode assemblies for water electrolysis, *ACS Appl Energy Mater*, 2020, **3**, 9635–9644.

30 S. Kole, G. Venugopalan, D. Bhattacharya, L. Zhang, J. Cheng, B. Pivovar and C. G. Arges, Bipolar membrane polarization behavior with systematically varied interfacial areas in the junction region, *J Mater Chem A Mater*, 2021, **9**, 2223–2238.

31 D. A. Vermaas, S. Wiegman, T. Nagaki and W. A. Smith, Ion transport mechanisms in bipolar membranes for (photo)electrochemical water splitting, *Sustain Energy Fuels*, 2018, **2**, 2006–2015.

32 S. Chabi, A. G. Wright, S. Holdcroft and M. S. Freund, Transparent Bipolar Membrane for Water Splitting Applications, *ACS Appl Mater Interfaces*, 2017, **9**, 26749–26755.

33 S. Z. Oener, M. J. Foster and S. W. Boettcher, Accelerating water dissociation in bipolar membranes and for electrocatalysis, *Science (1979)*, 2020, **369**, 1099–1103.

34 F. G. Wilhelm, PhD Thesis, University of Twente, 2001.

35 C. Shen, R. Wycisk and P. N. Pintauro, High performance electrospun bipolar membrane with a 3D junction, *Energy Environ Sci*, 2017, **10**, 1435–1442.

36 Y. Chen, J. A. Wrubel, W. E. Klein, S. Kabir, W. A. Smith, K. C. Neyerlin and T. G. Deutsch, High-Performance Bipolar Membrane Development for Improved Water Dissociation, *ACS Appl Polym Mater*, 2020, **2**, 4559–4569.

37 W. J. van Egmond, M. Saakes, I. Noor, S. Porada, C. J. N. Buisman and H. V. M. Hamelers, Performance of an environmentally benign acid base flow battery at high energy density, *Int J Energy Res*, 2018, **42**, 1524–1535.

38 J. Xue, T. Wu, Y. Dai and Y. Xia, Electrospinning and electrospun nanofibers: Methods, materials, and applications, *Chem Rev*, 2019, **119**, 5298–5415.

39 E. Al-Dhubhani, H. Swart, Z. Borneman, K. Nijmeijer, M. Tedesco, J. W. Post and M. Saakes, Entanglement-Enhanced Water Dissociation in Bipolar Membranes with 3D Electrospun Junction and Polymeric Catalyst, *ACS Appl Energy Mater*, 2021, **4**, 3724–3736.

40 P. K. Giesbrecht and M. S. Freund, Recent Advances in Bipolar Membrane Design and Applications, *Chemistry of Materials*, 2020, **32**, 8060–8090.

41 R. Pärnamäe, S. Mareev, V. Nikonenko, S. Melnikov, N. Sheldeshov, V. Zabolotskii, H. V. M. Hamelers and M. Tedesco, Bipolar membranes: A review on principles, latest developments, and applications, *J Memb Sci*, 2021, **617**, 118538.

42 G. Decher, Fuzzy nanoassemblies: Toward layered polymeric multicomposites, *Science (1979)*, 1997, **277**, 1232–1237.

43 S. T. Dubas and J. B. Schlenoff, Factors controlling the growth of polyelectrolyte multilayers, *Macromolecules*, 1999, **32**, 8153–8160.

44 S. Abdu, K. Sricharoen, J. E. Wong, E. S. Muljadi, T. Melin and M. Wessling, Catalytic polyelectrolyte multilayers at the bipolar membrane interface, *ACS Appl Mater Interfaces*, 2013, **5**, 10445–10455.

45 S. Chabi, K. M. Papadantonakis, N. S. Lewis and M. S. Freund, Membranes for artificial photosynthesis, *Energy Environ Sci*, 2017, **10**, 1320–1338.

46 N. Li and M. D. Guiver, Ion Transport by Nanochannels in Ion-Containing Aromatic Copolymers, *Macromolecules*, 2014, **47**, 2175–2198.

47 H. Strathmann, A. Grabowski and G. Eigenberger, Ion-Exchange Membranes in the Chemical Process Industry, *Ind Eng Chem Res*, 2013, **52**, 10364–10379.

48 J. Ran, L. Wu, Y. He, Z. Yang, Y. Wang, C. Jiang, L. Ge, E. Bakangura and T. Xu, Ion exchange membranes: New developments and applications, *J Memb Sci*, 2017, **522**, 267–291.

49 F. G. Wilhelm, I. Pünt, N. F. A. Van Der Vegt, M. Wessling and H. Strathmann, *Optimisation strategies for the preparation of bipolar membranes with reduced salt ion leakage in acid-base electrodialysis*, 2001, vol. 182.

50 B. Bauer, F. J. Gerner and H. Strathmann, *Development of Bipolar Membranes**, 1988, vol. 68.

51 H. Strathmann, H.-J. Rapp, B. Bauer and C. M. Bell, Theoretical and practical aspects of preparing bipolar membranes, *Desalination*, 1993, **90**, 303–323.

52 S. A. Mareev, E. Evdochenko, M. Wessling, O. A. Kozaderova, S. I. Niftaliev, N. D. Pismenskaya and V. V. Nikonenko, A comprehensive mathematical model of water splitting in bipolar membranes: Impact of the spatial distribution of fixed charges and catalyst at bipolar junction, *J Memb Sci*, , DOI:10.1016/j.memsci.2020.118010.

53 R. Simons, Water splitting in ion exchange membranes, *Electrochim Acta*, 1985, **30**, 275–282.

54 S. Mafé and P. Ramfaz, Electrochemical characterization of polymer ion-exchange bipolar membranes, *Acta Polymerica*, 1997, **48**, 234–250.

55 V. Kaiser, S. T. Bramwell, P. C. W. Holdsworth and R. Moessner, Onsager's Wien effect on a lattice, *Nat Mater*, 2013, **12**, 1033–1037.

56 I. C. Bassignana and H. Reiss, Ion transport and water dissociation in bipolar ion exchange membranes, *J Memb Sci*, 1983, **15**, 27–41.

57 L. Onsager, Deviations from Ohm's law in weak electrolytes, *J Chem Phys*, 1934, **2**, 599–615.

58 S. Mafé and P. Ramírez, Electrochemical characterization of polymer ion-exchange bipolar membranes, *Acta Polymer.*, 1997, **48**, 234–250.

59 S. Mafé, P. Ramírez and A. Alcaraz, Electric field-assisted proton transfer and water dissociation at the junction of a fixed-charge bipolar membrane, *Chem Phys Lett*, 1998, **294**, 406–412.

60 J. J. Krol, M. Jansink, M. Wessling and H. Strathmann, Behaviour of bipolar membranes at high current densityWater diffusion limitation, *Sep Purif Technol*, 1998, **14**, 41–52.

61 H. Strathmann, J. J. Krol, H.-J. Rapp and G. Eigenberger, Limiting current density and water dissociation in bipolar membranes, *J Memb Sci*, 1997, **125**, 123–142.

62 V. Zabolotskii, N. Sheldeshov and S. Melnikov, Heterogeneous bipolar membranes and their application in electrodialysis, *Desalination*, 2014, **342**, 183–203.

63 J. Balster, S. Srinkantharajah, R. Sumbharaju, I. Pünt, R. G. H. Lammertink, D. F. Stamatialis and M. Wessling, Tailoring the interface layer of the bipolar membrane, *J Memb Sci*, 2010, **365**, 389–398.

64 Z. Yan, L. Zhu, Y. C. Li, R. J. Wycisk, P. N. Pintauro, M. A. Hickner and T. E. Mallouk, The balance of electric field and interfacial catalysis in promoting water dissociation in bipolar membranes, *Energy Environ Sci*, 2018, **11**, 2235–2245.

65 L. Chen, Q. Xu, S. Z. Oener, K. Fabrizio and S. W. Boettcher, Design principles for water dissociation catalysts in high-performance bipolar membranes, *Nat Commun*, 2022, **13**, 3846.

66 R. Simons, Preparation of a high performance bipolar membrane, *J Memb Sci*, 1993, **78**, 13–23.

67 N. Ohmura, S. Tanaka, T. Soda, K. Kaisha and J. Tokuyama, Bipolar membrane and method for its production, *Patent 5,221,455*.

68 R. Simons and G. Khanarian, Water dissociation in bipolar membranes: Experiments and theory, *J Membr Biol*, 1978, **38**, 11–30.

69 FumaTech BWT GmbH, Technical Data Sheet - fumion FAA-3 shredded film, https://www.bwt.com/en/-/media/bwt/fumatech/datasheets/new/fumion/fumion-faa-3-shredded-film.pdf?rev=35904cd7e67944a38279064513d904ff, (accessed 21 March 2023).

70 J. De Grooth, M. Dong, W. M. De Vos and K. Nijmeijer, Building polyzwitterion-based multilayers for responsive membranes, *Langmuir*, 2014, **30**, 5152–5161.

71 J. de Grooth, R. Oborný, J. Potreck, K. Nijmeijer and W. M. de Vos, The role of ionic strength and odd-even effects on the properties of polyelectrolyte multilayer nanofiltration membranes, *J Memb Sci*, 2015, **475**, 311–319.

72 D. Scheepers, B. Chatillon, K. Nijmeijer and Z. Borneman, Asymmetric layer-by-layer polyelectrolyte nanofiltration membranes with tunable retention, *Journal of Polymer Science*, 2021, **59**, 1293–1304.

73 D. Scheepers, B. Chatillon, Z. Borneman and K. Nijmeijer, Influence of charge density and ionic strength on diallyldimethylammonium chloride (DADMAC)-based polyelectrolyte multilayer membrane formation, *J Memb Sci*, , DOI:10.1016/j.memsci.2020.118619.

74 D. Scheepers, J. de Keizer, Z. Borneman and K. Nijmeijer, The pH as a tool to tailor the performance of symmetric and asymmetric layer-by-layer nanofiltration membranes, *J Memb Sci*, , DOI:10.1016/j.memsci.2022.121320.

75 P. Bertrand, A. Jonas, A. Laschewsky and R. Legras, Ultrathin polymer coatings by complexation of polyelectrolytes at interfaces: Suitable materials, structure and properties, *Macromol Rapid Commun*, 2000, **21**, 319–348.

76 J. de Grooth, PhD Thesis, University of Twente, 2015.

77 Y. Fu, S. J. Li, J. Xu, M. Yang, J. D. Zhang, Y. H. Jiao, J. C. Zhang, K. Zhang and Y. G. Jia, Facile and efficient approach to speed up layer-by-layer assembly: Dipping in agitated solutions, *Langmuir*, 2011, **27**, 672–677.

78 K. Fujimoto, S. Fujita, B. Ding and S. Shiratori, Fabrication of layer-by-layer self-Assembly films using roll-to-roll process, *Japanese Journal of Applied Physics, Part 2: Letters*, , DOI:10.1143/JJAP.44.L126.

79 K. Fujimoto, J. H. Kim and S. Shiratori, Characterization of self-assembled flexible multilayer electrode film by roll-to-roll process, *Jpn J Appl Phys*, 2008, **47**, 8644–8647.

80 S. T. Dubas and J. B. Schlenoff, Swelling and smoothing of polyelectrolyte multilayers by salt, *Langmuir*, 2001, **17**, 7725–7727.

81 G. Decher, J. D. Hong and J. Schmitt, Buildup of ultrathin multilayer films by a self-assembly process: III. Consecutively alternating adsorption of anionic and cationic polyelectrolytes on charged surfaces, *Thin Solid Films*, 1992, **210–211**, 831–835.

82 K. Lowack and C. A. Helm, Molecular Mechanisms Controlling the Self-Assembly Process of Polyelectrolyte Multilayers, *Macromolecules*, 1998, **31**, 823–833.

83 C. B. Bucur, Z. Sui and J. B. Schlenoff, Ideal mixing in polyelectrolyte complexes and multilayers: Entropy driven assembly, *J Am Chem Soc*, 2006, **128**, 13690–13691.

84 J. Fu and J. B. Schlenoff, Driving Forces for Oppositely Charged Polyion Association in Aqueous Solutions: Enthalpic, Entropic, but Not Electrostatic, *J Am Chem Soc*, 2016, **138**, 980–990.

85 D. Bütergerds, C. Kateloe, C. Cramer and M. Schönhoff, Influence of the degree of ionization on the growth mechanism of poly(diallyldimethylammonium)/poly(acrylic acid) multilayers, *J Polym Sci B Polym Phys*, 2017, **55**, 425–434.

86 R. Steitz, W. Jaeger and R. v. Klitzing, Influence of charge density and ionic strength on the multilayer formation of strong polyelectrolytes, *Langmuir*, 2001, **17**, 4471–4474.

87 Z. Adamczyk, K. Jamrozy, P. Batys and A. Michna, Influence of ionic strength on poly(diallyldimethylammonium chloride) macromolecule conformations in electrolyte solutions, *J Colloid Interface Sci*, 2014, **435**, 182–190.

88 Z. Adamczyk, B. Jachimska, T. Jasiński, P. Warszyński and M. Wasilewska, Structure of poly (sodium 4-styrenesulfonate) (PSS) in electrolyte solutions: Theoretical modeling and measurements, *Colloids Surf A Physicochem Eng Asp*, 2009, **343**, 96–103.

89 L. Krasemann and B. Tieke, Highly efficient composite membranes for ethanol-water pervaporation, *Chem Eng Technol*, 2000, **23**, 211–213.

90 C. Naas, U. Scheler and U. Lappan, Influence of pH on the Growth and the Local Dynamics of Polyelectrolyte Multilayers, *Macromolecules*, 2021, **54**, 1043–1051.

91 J. C. Dijt, M. A. C. Stuart, J. E. Hofman and G. J. Fleer, Kinetics of polymer adsorption in stagnation point flow, *Colloids and Surfaces*, 1990, **51**, 141–158.

92 D. Kovacevic, S. Van der Burgh, A. De Keizer and M. A. Cohen Stuart, Kinetics of formation and dissolution of weak polyelectrolyte multilayers: Role of salt and free polyions, *Langmuir*, 2002, **18**, 5607–5612.

93 J. Fu, H. M. Fares and J. B. Schlenoff, Ion-Pairing Strength in Polyelectrolyte Complexes, *Macromolecules*, 2017, **50**, 1066–1074.

94 G. Ladam, P. Schaad, J. C. Voegel, P. Schaaf, G. Decher and F. Cuisinier, In Situ Determination of the Structural Properties of Initially Deposited Polyelectrolyte Multilayers, *Langmuir*, 2000, **16**, 1249–1255.

95 L. Wågberg, G. Pettersson and S. Notley, Adsorption of bilayers and multilayers of cationic and anionic co-polymers of acrylamide on silicon oxide, *J Colloid Interface Sci*, 2004, **274**, 480–488.

96 C. Picart, J. Mutterer, L. Richert, Y. Luo, G. D. Prestwich, P. Schaaf, J.-C. Voegel and P. Lavalle, Molecular basis for the explanation of the exponential growth of polyelectrolyte multilayers, *Proceedings of the National Academy of Sciences*, 2002, **99**, 12531–12535.

97 W. Yuan, Z. Lu and C. M. Li, Charged drug delivery by ultrafast exponentially grown weak polyelectrolyte multilayers: amphoteric properties, ultrahigh loading capacity and pH-responsiveness, *J Mater Chem*, 2012, **22**, 9351.

98 Y. Liao, R. Wang, M. Tian, C. Qiu and A. G. Fane, Fabrication of polyvinylidene fluoride (PVDF) nanofiber membranes by electro-spinning for direct contact membrane distillation, *J Memb Sci*, 2013, **425–426**, 30–39.

99 H. Liu, C. R. Gough, Q. Deng, Z. Gu, F. Wang and X. Hu, Recent Advances in Electrospun Sustainable Composites for Biomedical, Environmental, Energy, and Packaging Applications, *Int J Mol Sci*, 2020, **21**, 4019.

100 X. Zong, K. Kim, D. Fang, S. Ran, B. S. Hsiao and B. Chu, Structure and process relationship of electrospun bioabsorbable nanofiber membranes, *Polymer (Guildf)*, 2002, **43**, 4403–4412.

101 M. Halabi, M. Mann-Lahav, V. Beilin, G. E. Shter, O. Elishav, G. S. Grader and D. R. Dekel, Electrospun Anion-Conducting Ionomer Fibers—Effect of Humidity on Final Properties, *Polymers (Basel)*, 2020, **12**, 1020.

102 Z. Ge, M. A. Shehzad, X. Yang, G. Li, H. Wang, W. Yu, X. Liang, X. Ge, L. Wu and T. Xu, High-performance bipolar membrane for electrochemical water electrolysis, *J Memb Sci*, , DOI:10.1016/j.memsci.2022.120660.

103 P. DLUGOLECKI, K. NYMEIJER, S. METZ and M. WESSLING, Current status of ion exchange membranes for power generation from salinity gradients, *J Memb Sci*, 2008, **319**, 214–222.

104 E. and S. H. Giorno Lidietta and Drioli, in *Encyclopedia of Membranes*, ed. L. Drioli Enrico and Giorno, Springer Berlin Heidelberg, Berlin, Heidelberg, 2016, pp. 1490–1493.

105 B. Yuzer, H. Selcuk, G. Chehade, M. E. Demir and I. Dincer, Evaluation of hydrogen production via electrolysis with ion exchange membranes, *Energy*, 2020, **190**, 116420.

106 D. Henkensmeier, M. Najibah, C. Harms, J. Žitka, J. Hnát and K. Bouzek, Overview: State-of-the Art Commercial Membranes for Anion Exchange Membrane Water Electrolysis, *Journal of Electrochemical Energy Conversion and Storage*, , DOI:10.1115/1.4047963.

Appendix A

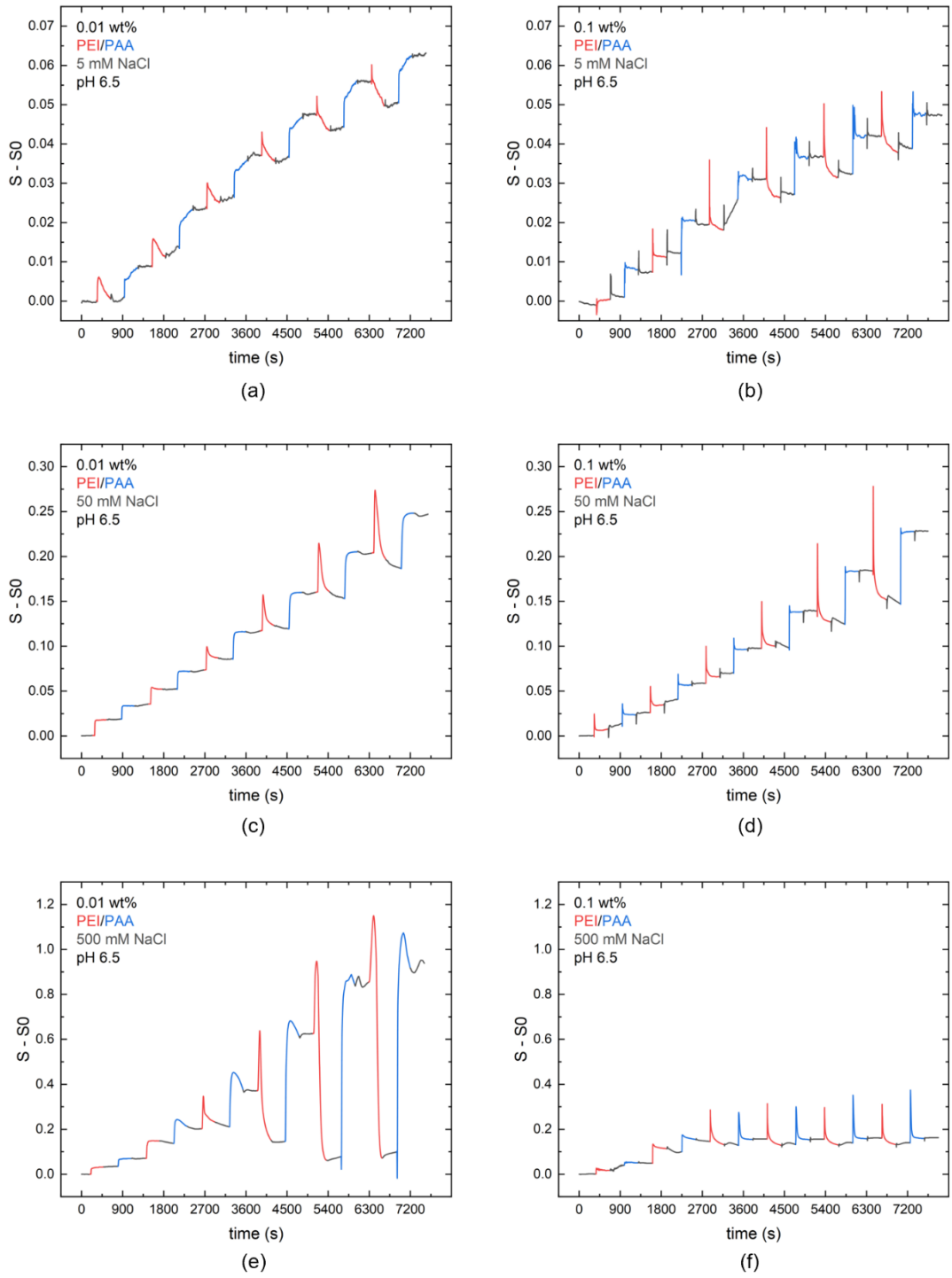

Figure A-1 Reflectometry signal versus time for six bilayers of 0.01 wt% (a, c, e) and 0.1 wt% (b, d, f) PEI and PAA at 5, 50 and 500 mM NaCl at a pH of 6.5.

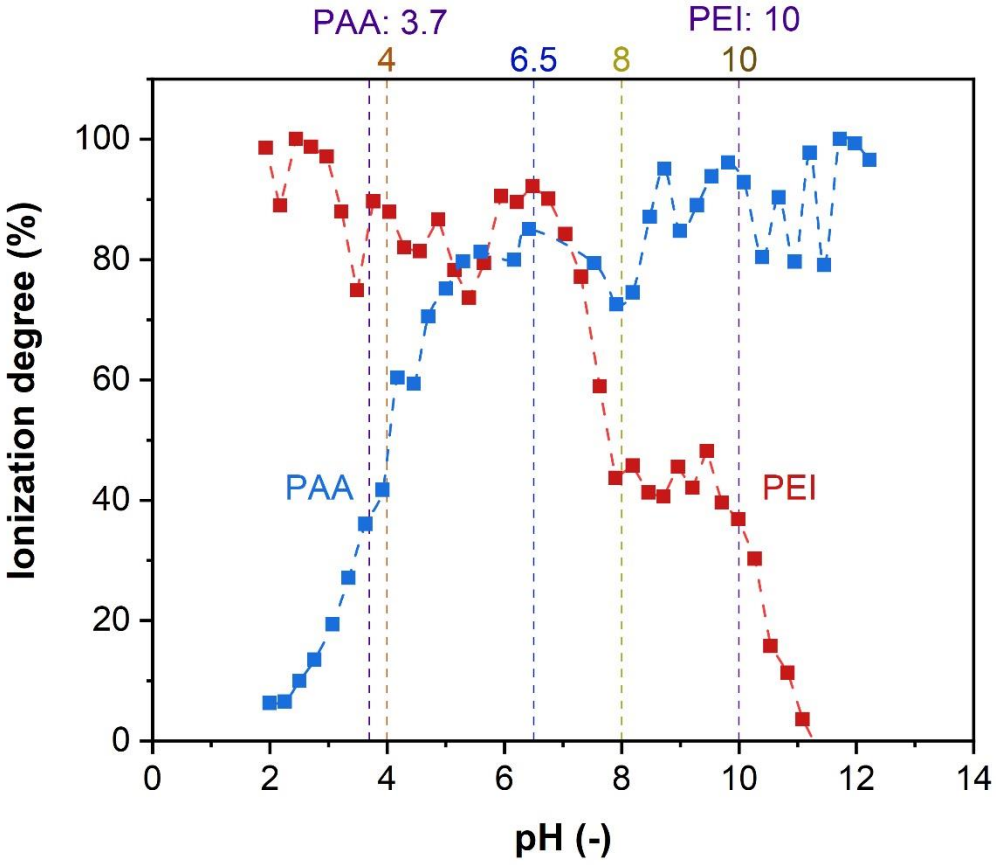

Figure A-2 Ionization degree (α) of PEI and PAA as a function of pH as determined by zeta potential measurements. The vertical dashed lines indicate the pH of the coating solutions used during reflectometry experiments.

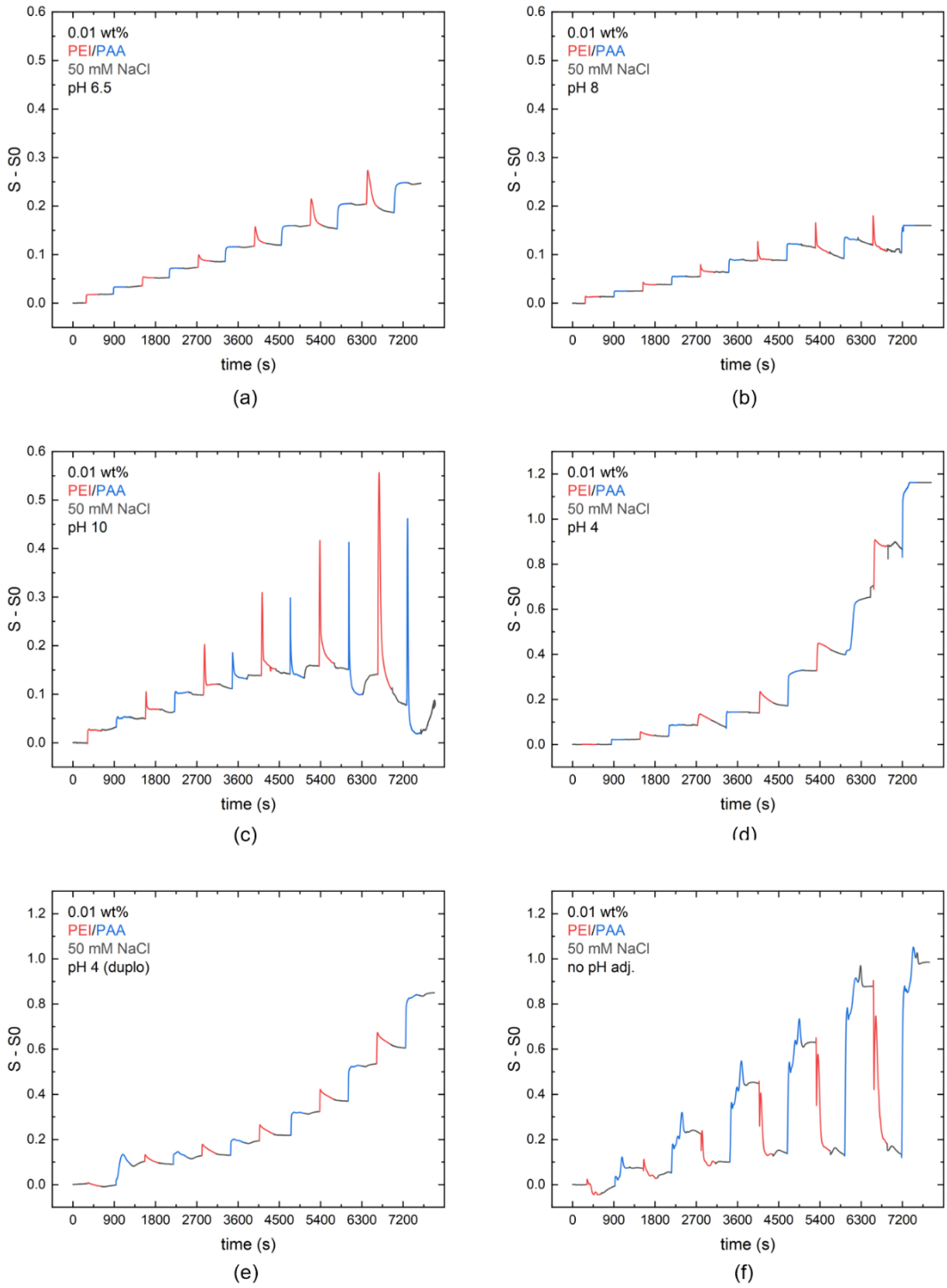

Figure A-3 Reflectometry signal versus time for six bilayers of 0.01 wt% PEI and PAA at 50 mM NaCl and (a) pH 10, (b) pH 8, (c & d) pH 4 and (e) pH_{PEI} = 10, pH_{PAA} = 3.7, $pH_{solvent}$ = 5.8.

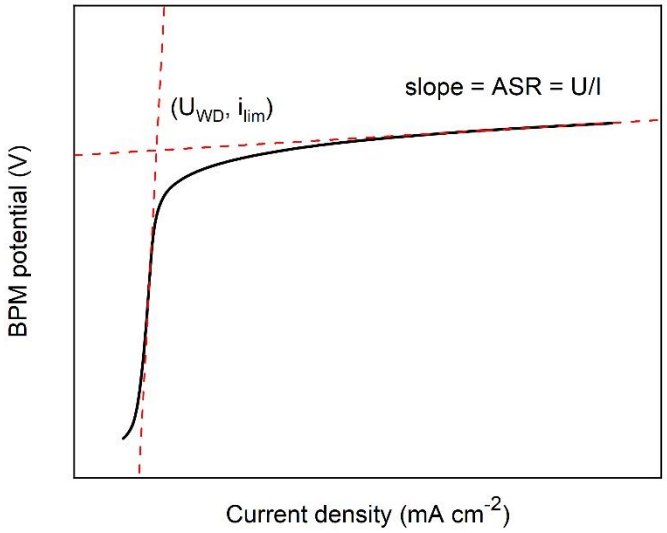

Figure A-4 Example of how the area specific resistance (ASR=U/I), the water dissociation onset potential (U_{WD}) and the limiting current density (i_{lim}) are determined from a polarization curve.

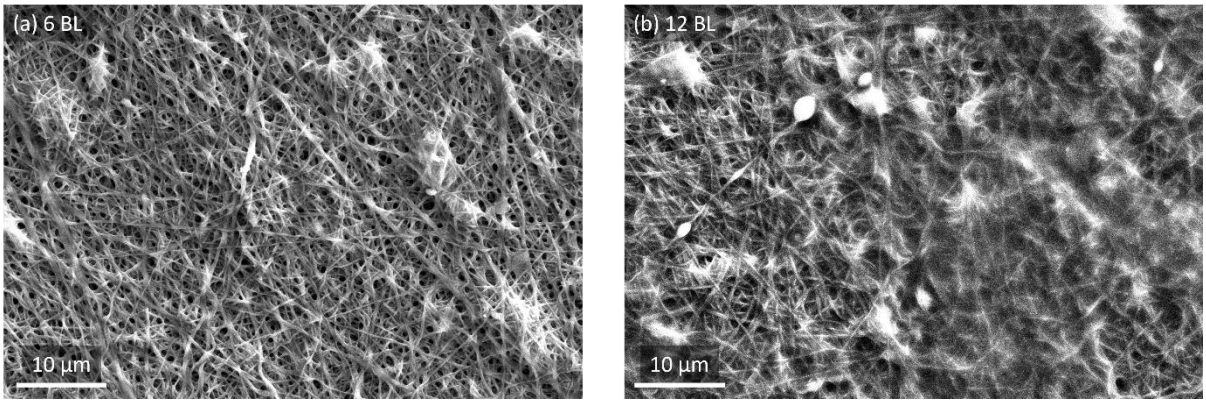

Figure A-5 SEM images of LbL coated electrospun SPEEK with (a) 6 BL and (b) 12 BL of 0.01 wt% PEI and PAA in 500 mM NaCl at pH 6.5.